Alma Mater Studiorum – Università di Bologna

DOTTORATO DI RICERCA IN FISICA

Ciclo XXVIII

Settore Concorsuale di afferenza: 02/D1
Settore Scientifico disciplinare: FIS/07

TIME DOMAIN AND SPATIALLY RESOLVED NMR: ADVANCED APPLICATIONS TO POROUS MEDIA OF INTEREST TO ENVIRONMENTAL SUSTAINABILITY AND HUMAN HEALTHCARE

Presentata da Leonardo Brizi

Coordinatore Dottorato — Prof. Gastone Castellani

Relatore — Prof.ssa Paola Fantazzini

Esame finale anno 2016

To Sara…

SUMMARY

LIST OF FIGURES

1 INTRODUCTION

The research performed during the three years of PhD study at the Department of Physics and Astronomy (DIFA) of the University of Bologna is part of a long-term project developed at the Nuclear Magnetic Resonance (NMR) Laboratory of this department, which goal is the advancement of theoretical approaches, methodologies, algorithms, and applications of Magnetic Resonance for fluids in Porous Media (shortly MRPM) [1].
The MRPM Community is now a vast community of scientists from all over the world, who recognize in Magnetic Resonance an instrument of choice for the characterization of porous media and of fluids inside in a vast range of different materials. The scene was different in 1990, when a series of conferences on these themes was promoted at the University of Bologna. Now this conference series is called International Bologna MRPM conferences and is spread all over the world; after being held in many countries in Europe, USA and New Zealand, the 13th edition will turn back to Bologna in September 2016.

One can say that now MRPM studies have acquired the dignity of a new interdisciplinary discipline.

Now, MRPM methodologies have become increasingly important tools to investigate pore space as well as surface and fluid properties in a wide class of heterogeneous high surface-to-volume ratio systems, of natural or synthetic origin, of organic or inorganic nature. Porous rocks, porcelains, zeolites, colloids, emulsions, gels, suspensions, as well as biological systems as bones, cartilage, cells and foods are in the mainstream of materials studied [2]–[5]. Structure, fluid-flow properties, water absorption, water diffusion and exchange among compartments are typical phenomena examined.

This thesis is an example of the different fields in which the same techniques, methods of data acquisition and algorithms for data analysis can be applied to get unique information, from system characterized by a wide range of scale lengths, which in some cases can span from a few nanometers to the macroscale level, and by compartments in which water can be confined under different regimes of diffusion and exchange.

From the beginning, these techniques and interpretation models were applied to both solid porous media and biological systems that, for many aspects, can be considered as porous media. In this thesis the same methods of data tacking and analysis will be applied to both rocks and biological systems. The biological systems will be solid porous media, as bone and corals, but also human cells.

The growth of MRPM from the end of the 1940s was bound for years to the development in oil industry of Nuclear Magnetic well Logging (NML) projects. The idea on the basis of these projects was to detect the NMR signal of oil and water down in the oil-wells at the depth of thousands of meters, to evaluate the fraction oil-to-water in the pore space of the rock formation around the well. In these first works the origin can be found of

techniques later developed for applications other than well logging or petrophysical studies, that is, field-cycling and ex-situ techniques. This last technique allows one to get NMR signal from samples placed outside the magnet. Part of this thesis will be devoted to apply this technique.

The MRPM work at Bologna began in the mid-eighties. New correlations were found among parameters from NMR relaxation measurements and such oilfield parameters as porosity, permeability to fluid flow, irreducible water saturation, residual oil saturation, and surface-to-volume ratio, and fast algorithms were developed to give the different NMR parameters. Interest in valid interpretation of data led to extensive work also on the inversion of multiexponential relaxation data and the effects of inhomogeneous fields from susceptibility differences on distributions of relaxation times. In the last few years extensive developments were made of combined magnetic resonance imaging and relaxation measurements in different fields [1].

The last advancements, object of this thesis, regard measurements in highly homogeneous magnetic fields and in the presence of the magnetic field gradient of single-sided devices. The experiments performed are single and multi-dimensional NMR experiments. In particular, during this thesis project two-dimensional correlation analyses have been settled and exploited, including relaxation-relaxation, relaxation-diffusion, relaxation exchange. These techniques allow one to study surface-to-volume, tortuosity and connectivity in solid porous media and water exchange and compartmentation in cells.

The most important MRPM techniques applied in this thesis are Relaxometry, Diffusometry and Imaging (MRI) of ^{1}H nuclei of liquid water confined inside the pore space of the porous material. Everybody knows MRI, due to the huge impact it has had

on medicine, thanks to its impressive diagnostic power. Nevertheless, very few experts know that MRI can be applied to visualize in a non-destructive manner internal sections of porous media saturated with water [6], with the possibility of 3D reconstructions of the structure of the pore space occupied by water. While imaging allows one to get information at the sample-scale, relaxation data give information at the pore-scale. Relaxometry and MRI can be combined in Relaxation-Imaging, which allows the spatially-resolved study of NMR parameters connected with the pore space. Diffusometry allows one to measure apparent self-diffusion coefficient of water inside the pore space, and measurements performed allowing increasing diffusion times allow one to determine surface-to-volume ratio and tortuosity of the pores. Measurements allowing for increasing exchange time allow one to determine connectivity among pores. These techniques are also applicable by means of portable instruments or instruments that can in any case be transported for measurements in situ.

A part of this thesis is devoted to Cultural Heritage applications. Until recent years no one would have thought of employing NMR techniques for materials and objects of historical-artistic-archaeological interest. This was true because for the study of materials people thought mainly of NMR Spectroscopy, a technique for high resolution in chemistry. The scene changed when it was thought to apply to Cultural Heritage the wealth of knowledge and technology developed in the field of MRPM, that can now be profitably applied to the preservation of the Cultural Heritage [7] for both laboratory research and in situ diagnosis on porous media like rocks, ornamental stones, bricks, cements, mortars, wood. What makes MRPM appealing for Cultural Heritage is the capability of probing in non-destructive and non-invasive manner water molecules inside

the pore space [8]. It is well known that water is the main deterioration agent for porous materials, in which gases and water can diffuse from the environment. This gives rise to the dissolution of the binder and the creation of internal mechanical stresses. Water also dissolves pollutants from the atmosphere, causing acidic corrosion of stone. Quantitative measurement of the moisture contained in a porous material and of lengths characteristic of the pore space can be analyzed before and after treatment with protective and/or consolidative product, and followed in time, in such a way that they can furnish information useful for diagnosis and therefore for planning the most appropriate conservation, restoration, and maintenance procedures. The results presented in this thesis demonstrate the great advancements that MRPM can determine, as compared to the traditional methods, in the study of the water-surface interactions in the presence of conservative products, their uniform or non-uniform distribution inside the samples, the efficacy of protective and consolidative treatments. This research has been performed in collaboration with the "Istituto di Geologia e Georisorse – CNR" of Florence, and in Germany in collaboration with the research group at the Department of Macromolecular Chemistry of the RWTH University of Aachen.

The same techniques applied to stones of interest to cultural heritage can be applied to other porous media. In this thesis they have been applied to the skeletons of corals and human (or animal) bones. They are solid porous media, with a multi-scale length of pore sizes. If the pore space is saturated with fluids containing ^{1}H nuclei, MRPM methods allow one to quantify the porosity at different scale lengths.

In the case of the coral skeletons, important correlations have been found between the porosity at the macroscale and the level of acidity of the sea water when the corals have

grown. Important conclusions have been drown about a possible acclimation process of the corals in a world subjected to climate change, with ocean warming and acidification, This research has been performed in collaboration with the group of Marine-Biology of the Department BiGEA (University of Bologna).

In the case of bones, the goal of the project was to propose and test an innovative and non-invasive procedure for the diagnosis of osteoporosis by means of a portable, low-cost, low field NMR instrument. The results show that the values of an important parameter, the bone volume-to-total volume ratio, determined with the proposed procedure are consistent with the values obtained for comparison with μCT analysis. This research has been performed in collaboration with the "Laboratorio di Tecnologie Biomediche - Istituto Ortopedico Rizzoli" of Bologna.

For the analysis of bones, as well for the samples examined for the research on Cultural Heritage, NMR single-sided instruments have been utilized.

For some aspects, also cells can be considered as "porous media", even if in this case there are not solid surface to confine water, but membranes. The relaxometry can be used to detect the changes of the cellular environments and the water compartmentalization. In this thesis results are reported of the analysis of changes of a cellular population under stress. The behavior of the NMR signals (in terms of relaxation times and relative signal fractions) allowed us to distinguish three phases, consistent with the results of optical microscopy analyses. This research has been performed in collaboration with the group of Biophysics of the Department of Physics and Astronomy of the University of Bologna.

In summary, time-domain and spatially resolved NMR techniques developed in the field of Magnetic Resonance for fluids in Porous Media have been successfully applied to study various porous systems of different nature and origin, containing hydrogenous fluids. The unifying principle of this work is showing how the NMR analyses performed with these techniques can be extended to a multiplicity of porous material and how these methods are able to investigate the structure of the pore space and other features in a non-destructive manner, on the intact sample, from the macroscopic scale to the nanometric one. Moreover, the results of this thesis demonstrate that the same experimental NMR procedures can be successfully applied to perform researches in important topics that deal with the *Sustainability of Environment and Human Healthcare.*

An important part of my work during the PhD, beside contributing to the planning of the experiments, to data acquisition and interpretation, has been devoted to: (i) the implementation of the technology of multi-dimensional data acquisition and analysis at the NMR laboratory of the Department DIFA; (2) the setup of the single-sided NMR instrument, constituted by the NMR MOUSE, the lift for its automatic movement, and the console for NMR experiment acquisition. An important experience on the use of this instrument has been acquired during my research period (6 months) spent in Germany (University of Aachen and Forschungszentrum of Jülich).

This thesis consists of 6 chapters. The first one is this Introduction. In the second chapter the theory of mono and multi-dimensional time-domain NMR is exposed. The third chapter describes the experimental setups and instruments used. The fourth chapter is

related to the researches devoted to the Environment Sustainability, the fifth to the Human Healthcare. In the last chapter the conclusions are summarized.

2 NUCLEAR MAGNETIC RESONANCE IN POROUS MEDIA

The physical phenomenon of ^{1}H Nuclear Magnetic relaxation, in molecular fluids, is mostly caused by dipolar interactions between nuclear spin of nuclei that constitute the fluid. In various hydrogenous liquids, the main source of relaxation is the dipolar relaxation of protons of the same molecule. Usually small molecules (in this case water molecules) are characterized by a fast rotational diffusion that makes the correlation time short and thus the relaxation is weak. In this chapter, relaxation and diffusion processes of hydrogenous fluid confined in porous media are discussed.

2.1 Relaxation of fluids in porous media

NMR relaxation and diffusion are fundamental phenomena for investigating the dynamics of nuclei and their interaction with surrounding environment. In fluids that saturate porous media, some physical processes participate in the relaxation. The most significant contribution is related to the diffusion at the surface of pores, where spins experience relaxation at the boundary of liquid-solid [9], [10]. In order to describe this behavior, the surface relaxivity parameter ρ, related to properties of the solid matrix and of the fluid at

the solid-liquid interface, is considered. The so called surface relaxation is the physical phenomenon that characterized the interaction between the solid surface and the molecular fluid [11].

Considering a fully saturated pore of volume V_p, with a surface layer of liquid of thickness d and volume $V_L = dS$, where S is the total surface of the pore, the effective relaxation is an average between the contribution of the bulk and the surface, since the water molecule moves between the bulk volume of the pore and the thin layer at the surface. Relaxation parameters $T_{1,2}$ are described by the following equation:

$$\frac{1}{T_{1,2}} = \frac{1}{T_{1b,2b}} + \frac{d \cdot S}{V_P} \cdot \frac{1}{T_{1s,2s}} \qquad \textit{Eq. 1}$$

Where indexes *b* denotes the bulk relaxation and *s* the relaxation at the surface. Defining the surface relaxivity $\rho_{1,2} \equiv d / T_{1s,2s}$ the above equation become the well-known equation:

$$\frac{1}{T_{1,2}} = \frac{1}{T_{1b,2b}} + \rho_{1,2} \cdot \frac{S}{V_P} \qquad \textit{Eq. 2}$$

with ρ_1 and ρ_2 surface relaxivity for T_1 and T_2 relaxation respectively. This relationship is justified by the assumption of fast diffusion according to which molecules diffuse quickly between the surface and the bulk volume. This assumption is valid in a wide class of porous media saturated with water as reported in literature [12], [13], [14], where the validity of this assumption is verified by the comparison between Mercury Injection Porosimetry (MIP) and NMR analyses.

2.2 Diffusion of fluids in porous media

The porous structure of the medium confines the motion of fluid molecules and often this feature determines a reduction of the measured diffusion coefficient $D(t)$ [15], called apparent diffusion coefficient, respect to its bulk value D_0. The bulk diffusion coefficient is an important parameter to describe the translational diffusion under the condition of random Brownian motion. The Einstein's definition is valid for times t much larger than times that characterize molecular collisions

$$\langle [r'(t) - r(0)]^2 \rangle = 2dim\, D_0\, t \qquad Eq.\ 3$$

Where <…> is the mean square displacement of diffusing molecules over all initial r(0) and final r'(t) positions, dim is the dimensionality of the system and 0 is the index of D for indicating the bulk condition.

In porous media, since the solid matrix is not permeable by water, the motion of fluid molecules is restricted. In particular, for an open porous material with interconnected pores, the apparent diffusion coefficient $D(t)$ shows two different behaviors depending on the time interval given to molecules for diffusing.

At short diffusion time [16], molecules diffuse a distance $(D_0\, t)^{1/2}$ that is comparable to the characteristic length scale of the pore and, for this reason, molecules are sensitive only to the confining geometry of the pore. The attenuation of the diffusion coefficient results to be

$$\frac{D(t)}{D_0} \approx 1 - A\sqrt{D_0\, t}\, \frac{S}{V_P} \qquad Eq.\ 4$$

Where A is a dimensionality constant ($A = \frac{4}{9\sqrt{\pi}}$ for spherical pores). The second behavior occurs when the diffusion mean square displacement is larger than the pore size. In this situation, if pores are well-connected, diffusing molecules move around the grains in such a way that the total distance in order to achieve a displacement *x* is larger than *x*. Thus, the reduction of *D*(*t*), at long diffusion time, approaches a constant value related to the tortuosity factor α according to the following equation:

$$\frac{D(t \to \infty)}{D_0} \approx \frac{1}{\alpha} \qquad \textit{Eq. 5}$$

For porous media saturated with fluids characterized by spherical pores interconnected, the attenuation of the diffusion coefficient follows the equation [17]:

$$\frac{D(t)}{D_0} = 1 - \frac{\frac{4\sqrt{D_0 t}}{9\sqrt{\pi}}\frac{S}{V_P} + \left(1 - \frac{1}{\alpha}\right)\frac{D_0 t}{D_0 \theta}}{\left(1 - \frac{1}{\alpha}\right) + \frac{4\sqrt{D_0 t}}{9\sqrt{\pi}}\frac{S}{V_P} + \left(1 - \frac{1}{\alpha}\right)\frac{D_0 t}{D_0 \theta}} \qquad \textit{Eq. 6}$$

Where θ is a fitting parameter with dimensions of time and it represents the typical time that the molecules need to diffuse a macroscopic distance *l* to reach the tortuosity limit [18] $\theta = l^2/D_0$.

2.3 Two-dimensional NMR

Usually, the one-dimensional NMR concerns an experiment in which signals are acquired as a function of a controlled variable parameter of the specific rf pulse sequence used. On

the contrary, the multi-dimensional NMR, in particular two-dimensional NMR, refers to an experiment performed by controlling two different variable parameters. In order to obtain the two-parameter correlation function, a two-dimensional Inverse Laplace Transform (ILT) is required. The two-dimensional NMR methods exploited in this thesis regard the following two correlation functions: Exchange-Relaxation (T_2-T_2) and Diffusion-Relaxation (D-T_2).

In a conventional 2D-NMR experiment, where the two dimensions are the parameters x and y, a data matrix M is sampled for variable times τ_1 and τ_2. The relationship between acquired data and the correlation function *F(x, y)* is given by a Fredholm integral of the first kind with the tensor product kernel:

$$M(\tau_1, \tau_2) = \iint F(x, y) k_1(x, \tau_1) k_2(y, \tau_2)\, dxdy \qquad \textit{Eq. 7}$$

Where k_1 and k_2 are continuous and smooth functions. For fluids in connected porous media, characterized by diffusion between pores, the diffusion phenomenon cannot be assumed as independent from relaxation and is described [19] by equation Eq. 8.

Indeed, the evolution of magnetization in the presence of diffusion and relaxation phenomena is described by the Bloch-Torrey equation [20]:

$$\frac{\delta}{\delta t} m(r, t) = D_0 \nabla^2 m(r, t) - \mu m(r, t) \qquad \textit{Eq. 8}$$

where μ is the bulk relaxation rate and m is the relative difference of the magnetization and its equilibrium. The acquired signal is $M(t) = \int m(r, t) dv$.

The general solution of the Eq. 8 can be written as a sum of eigenmodes:

$$m(r,t) = e^{-\mu t}\sum_{i=0}^{\infty} a_i e^{-\frac{t}{\tau_i}} \qquad \textit{Eq. 9}$$

where a_i are the weights of the eigenmodes in the magnetization, ϕ_i are normalized eigenfunctions and τ_i normalized eigenvalues. ϕ_i with $i \neq j$ are orthogonal and satisfy:

$$D_0 \nabla^2 \phi_i(r) + \frac{1}{\tau_i} = 0 \qquad \textit{Eq. 10}$$

with the boundary condition at the pore surface $D\hat{n}\cdot\nabla\phi_i + \rho\phi_i = 0$ where $\hat{n}$ is the unit vector normal to the pore surface *S*. Generally, the two eigensystems related to T_1 and T_2 processes are different because the surface relaxivity ρ assumes different values for T_1 and for T_2.

2.3.1 Relaxation correlation: T_1-T_2 relaxation-relaxation

The typical T_1-T_2 experiment uses the IR-CPMG as pulse sequence. In this case spins show two different dynamics. In the first period t_a, the magnetization evolves according to a T_1 process and it is described by L-modes. At the end of this period, the magnetization $m1(\boldsymbol{r},t_a)$ is

$$m1(\boldsymbol{r},t_a) = \sum_{i=0}^{\infty} a_i \phi_i^L(\boldsymbol{r}) e^{-\frac{t_a}{T_{1i}}} \qquad \textit{Eq. 11}$$

where a_i is determined by the magnetization at the end of the first π pulse, $m_0(r) = -1$. The second period starts with the π/2 pulse. The pulse rotates the magnetization to the transverse plane and the pin dynamics follows a T_2 process governed by T-modes. The CPMG echo signal, $m(\boldsymbol{r},t_a,t_b)$, evolves according the Eq.12.

$$m(\boldsymbol{r}, t_a, t_b) = \sum_{j=0}^{\infty} b_j \phi_j^T(\boldsymbol{r}) e^{-\frac{t_b}{T_{2j}}} \qquad Eq.\ 12$$

where $b_j = \int m1(\boldsymbol{r}, t_a)\phi_j^T(\boldsymbol{r})dv$. In the time-domain, the signal is the integral of the magnetization:

$$S(t_a, t_b) = \int m(\boldsymbol{r}, t_a, t_b)dv = \sum_{i,j} s_{ij} e^{-\frac{t_a}{T_{1i}} - \frac{t_b}{T_{2j}}} \qquad Eq.13$$

Using the notation $\langle \phi_j | \psi_i \rangle = \int \phi_j^* \psi_i dv$, where ϕ_j^* is the complex conjugate of ϕ_j, $s_{ij} = \langle \phi_j^T | 1 \rangle \langle \phi_j^T | \phi_i^L \rangle \langle \phi_i^L | 1 \rangle$. The $|1\rangle$ represents a constant function within the pore. After a Laplace inversion, the resulting spectrum is

$$s_{12}(T_2^b, \Delta, T_2^a) = \sum_{i,j,r} \langle 1 | \phi_i^T \rangle \langle \phi_i^T | \phi_r^L \rangle \langle \phi_r^L | 1 \rangle \times \delta(T_1 - T_{1,i})\, \delta(T_2 - T_{2,j}) \qquad Eq.14$$

Signals with i = j are called diagonal and with i ≠ j off-diagonal.

2.3.2 Relaxation correlation: T_2-T_2 exchange-relaxation

A T_2-T_2 experiment uses a pulse sequence composed by two CPMG with a time interval Δ interposed. During the time period t_a related to the first CPMG sequence, the magnetization dynamics is described by T-modes (ϕ_i^T). At the end of the period, the magnetization *m1(**r**, t_a)* results to be:

$$m1(\boldsymbol{r}, t_a) = \sum_{i=0}^{\infty} a_i \phi_i^T(\boldsymbol{r}) e^{-\frac{t_a}{T_{2i}}} \qquad Eq.\ 15$$

After the time interval Δ, where the magnetization relaxes according to the T_1 process, another train of CPMG pulses is used for acquiring data. The evolution of the detected signal *m(**r**, t_a, t_b)* is:

$$m(\boldsymbol{r}, t_a, t_b) = \sum_{j=0}^{\infty} b_j \phi_j^T(\boldsymbol{r}) e^{-\frac{t_b}{T_{2j}}} \qquad Eq.\ 16$$

where $b_j = \int m1(\boldsymbol{r}, t_a)\phi_j^T(\boldsymbol{r})dv$. In the time-domain, the signal is the integral of the magnetization:

$$S(t_a, t_b) = \int m(\boldsymbol{r}, t_a, t_b)dv = \sum_{i,j} s_{ij} e^{-\frac{t_a}{T_{2i}} - \frac{t_b}{T_{2j}}} \qquad Eq.\ 17$$

Using the notation $\langle \phi_j | \psi_i \rangle = \int \phi_j^* \psi_i \, dv$, where ϕ_j^* is the complex conjugate of ϕ_j, $s_{ij} = \langle \phi_j^T | 1 \rangle \langle \phi_j^T | \phi_i^T \rangle \langle \phi_i^T | 1 \rangle$. The $|1\rangle$ represents a constant function within the pore.
After a Laplace inversion, the resulting spectrum is

$$s_{22}(T_2^b, \Delta, T_2^a) = \sum_{i,j,r} \langle 1|\phi_i^T\rangle\langle\phi_i^T|\phi_r^L\rangle\langle\phi_r^L| \quad \rangle\langle\phi_j^T|1\rangle e^{-\frac{\Delta}{T_{1r}}} \times \\ \times \qquad\qquad \times\ \delta(T_2^a - T_{2i})\,\delta(T_2^b - T_{2j}) \qquad \textit{Eq. 18}$$

During the period Δ, spins relax according to the T_1 process, thus, the magnetization dynamics is described by L-modes. When $\Delta = 0 \rightarrow \sum_r |\phi_r^L\rangle\langle\phi_r^L| = 1$ and the spectrum is

$$s_{22}(T_2^b, \Delta, T_2^a) = \sum_{p,q,r} \langle 1|\phi_p^T\rangle\langle\phi_q^T|1\rangle \times \delta(T_2^a - T_{2p})\,\delta(T_2^b - T_{2q}) \qquad \textit{Eq. 19}$$

and only diagonal signals survive. When Δ is long, the weight distribution is controlled by the non-orthogonality between ϕ_p^T and ϕ_q^T, and off-diagonal peaks appear in the resulting map.

Further details about the specific experiment performed in this thesis are discussed in the section 3.2.2.2.

2.3.3 Diffusion-relaxation (D-T_2)

The correlation function D-T_2 is often studied by the use of a STE-CPMG, a Stimulated Echo sequence followed by a CPMG sequence, with Pulsed Field Gradients (PFG). In this situation, the spin dynamics has two different behaviors. The first is encoded by the first gradient pulse and the second is decoded by a second identical gradient after a time interval Δ. Thus, the magnetization after the first gradient m1($\mathbf{r}$, τ_1) is

$$m1(r,\Delta,q) = \sum_{j=0}^{\infty} a_j \phi_j(r) e^{-iqr} e^{\frac{\Delta}{T_{1j}}} \qquad Eq.\ 20$$

where $a_j = \langle 1|e^{-i\boldsymbol{qr}}|\phi_j\rangle = \int e^{-i\boldsymbol{qr}}\,\phi_j(\boldsymbol{r})d\boldsymbol{r}$. T_1j corresponds to decay time constants and L-modes describe the magnetization. After a time interval Δ, a second identical gradient is pulsed. Then, the second part of the sequence is a CPMG, thus spins are governed by ϕ^{T} modes. The echo signal *m(**r**, Δ, t)* evolves according to

$$m(\boldsymbol{r},\Delta,t) = \sum_{j=0}^{\infty} b_j \phi_j^T(\boldsymbol{r}) e^{-\frac{t}{T_{2j}}} \qquad Eq.\ 21$$

where $b_j = \int m1(\boldsymbol{r},h,\boldsymbol{q})\phi_j^T(\boldsymbol{r})dv$. The resulting time-domain signal over the total volume is

$$S(\Delta,\boldsymbol{q},t) = \int m(\boldsymbol{r},\Delta,\boldsymbol{q})dv = \sum_{l,j} s_{lj}(\boldsymbol{q}) e^{-\frac{\Delta}{T_{1l}}-\frac{t}{T_{2j}}} \qquad Eq.\ 22$$

where $s_{lj}(q) = \langle 1|e^{i\boldsymbol{qr}}|\phi_l\rangle\langle\phi_l|e^{-i\boldsymbol{qr}}|\phi_j^T\rangle\langle\phi_j^T|1\rangle$.

Further details about the specific experiment performed for this thesis are discussed in the subsection 3.2.2.3.

2.4 Laplace Inversion

In NMR relaxometry and diffusometry most of data analyses are performed by the use of a Laplace inversion in order to obtain the distribution of relaxation times or diffusion parameters. This kind of inversion is ill-conditioned and small noise can drastically affect

the resulting distribution [21]. One of the most common way to solve this problem is described in this subchapter, where the essential mathematics for approaching the ILT problem is presented.

2.4.1 One-Dimensional Laplace Inversion

The one-dimensional Laplace inversion consist in the determination of the relaxation times distribution *A(T)* from the acquired dataset *M(τ)*, and $M(\tau) = \int e^{-\frac{\tau}{T}} A(T) dT + \varepsilon$, where T is the relaxation constant and ε is the noise. In discretized matrix form, the previous equation can be rewritten as

$$M = KA + E \qquad Eq.\ 23$$

M is the data vector and *N* the noise vector. Matrix *K* is the kernel and *A* is the discretized version of *A(T)*. Thus, *M* and *K* are known and the true solution *A* satisfies the criterion $\|M - KA\| < \sigma$, where $\| \|$ is the vector norm and σ is the variance of the noise. In the real case, several solutions satisfy the criterion. In order to find a unique solution a certain criterion is chosen (i.e. stability against noise) and a regularization method [22] is applied. A fit to the data is obtained through the minimization of the following expression:

$$\|M - KA\|^2 + \alpha \|A\|^2 \qquad Eq.\ 24$$

where the first term calculates the difference between the data and the fit, and the second is the regularization terms controlled by the parameter α. The regularization finds a

smooth solution with a small 2-norm $\| A^2 \|$. The minimization is usually accelerated by the use of Singular Value Decomposition (SVD) of the matrix *K*.

2.4.2 Two-Dimensional Laplace Inversion

Two-dimensional NMR experiments are performed by controlling two different parameters τ_1 and τ_2 of the pulse sequence. Most of sequences are designed in order to acquire data that exhibit a behavior described by the Eq. 7, where the kernel *k* is split into two independent components k_1 and k_2,

$$\mathrm{k}(\tau_1, \tau_2, \mathrm{x}, \mathrm{y}) = \mathrm{k}_1(\tau_1, \mathrm{x})\mathrm{k}_2(\tau_2, \mathrm{y})\,. \qquad \textit{Eq. 25}$$

Here x and y are the distribution parameters (T_1, T_2 and D). In this case, previous equation can be written in matrix notation as:

$$M = K_1 A K_2^T + E \qquad \textit{Eq. 26}$$

where *M* and *E* are two-dimensional data matrixes of data and noise, respectively. The elements of the kernel matrixes are defined by $(K_1)_{ij} = k_1(\tau_{1i}, x_{1j})$ and $(K_2)_{ij} = k_2(\tau_{2i}, x_{2j})$.

SVD of matrices K_1 and K_2 is performed to reduce their dimension. Then the minimization of

$$\|M - K_1 A K_2^T\|^2 + \alpha \|A\|^2 \qquad \textit{Eq. 27}$$

is calculated.

The tensor product nature of the kernel K is an advantage because for 2D NMR experiment sizes of K matrix make not possible the direct computation of the SVD. When the SVD is calculated for K_1 and K_2, the two-dimensional inversion problem (Eq. 26) is converted to the one-dimensional case (Eq. 23).

3 INSTRUMENTAL SETUPS

In this chapter NMR instruments and pulse sequences used for investigating porous media are described. During my doctorate I exploited the possibility to manage different instruments in NMR laboratories of Bologna (Department of Physics and Astronomy, Department DICAM, University of Bologna). This instruments are: a relaxometer based on a Jeol C-H 60 electromagnet, a tomograph based on the Artoscan permanent magnet and a NMR MOUSE Profile PM10. Moreover, I spent a period abroad, in Aachen and Jülich, Germany, where I had the opportunity to deepen my knowledge about single-sided NMR by the use of MOUSE Profile PM25 (Research Centre of Jülich). In the same Institute, I also realized MRI on a tomograph based on a Varian superconducting magnet.

3.1 Instruments

3.1.1 Single-Sided NMR: the MOUSE Profile

The NMR MOUSE (MObile Universal Surface Explorer) is a single-sided NMR instrument [23], [24]. Unilateral magnets are characterized by a strong magnetic field gradient G_0 perpendicular to the magnet surface. The Figure 3.1 depicts the basic operational principle of the instrument.

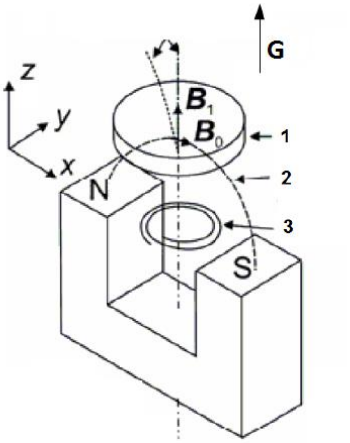

Figure 3.1 - Sketch of the operational principle of the MOUSE. (1) sensitive volume, (2) magnetic field B_0 and (3) the coil.

The radiofrequency coil, that generates the B_1 and acquires the relaxation signal, is located between the Northern and the Southern magnetic poles. The magnet is based on a U-shape geometry. In order to improve the constancy of the magnetic field gradient, the two magnets of the U-shape are split into four magnetic blocks. The sensitive volume is 17 mm x 17 mm in the XY plane for the MOUSE PM10 and 25 mm x 25 mm for the PM25. The thickness can be varied in the range 100-300 µm changing parameters as the pulse length and the acquisition sampling rate. Inside the sensitive volume, the magnetic field B_0 = 0.327 T for both the PM10 and the PM25, corresponding to a Larmor frequency for ^{1}H nuclei ν_0 = 13.9 MHz. The fundamental feature is the strong magnetic field gradient that is G_{010} = 14 T/m for the PM10 and G_{025} = 7 T/m for the PM25, as declared by the constructor.

An interesting feature concern the capability to vary the distance h of the coil respect to the sensitive volume through the insertion of spacers between the coil plate and the

surface of the magnet. For the PM10 the maximum value of h is h_{10} = 10 mm, while for PM25 h_{25} = 25 mm. The distance h allows to conduct NMR analyses inside a sample, just approaching the instrument to the sample, i.e. wall paintings [25], or just leaving the sample on the instrument plate.

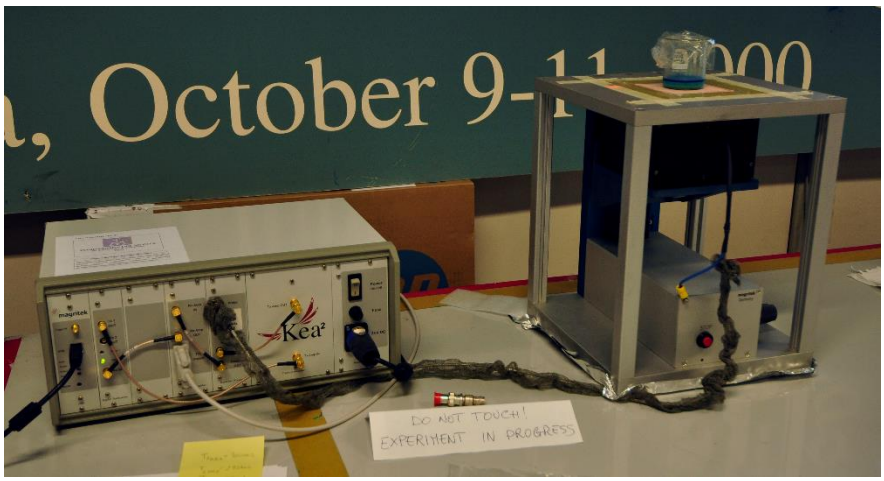

Figure 3.2: MOUSE PM10 mounted on a lift and KEA II spectrometer

Furthermore, exploiting this characteristic, it is possible to change the depth of the sensitive volume inside the sample. Useful information about NMR parameters can be acquired as functions of the depth by repeating NMR experiments at different position inside the sample. With the use of a high-precision automated lift, piloted by the Prospa software, it is possible to move the MOUSE for steps of order of micrometers. In this way, the single-sided apparatus can acquire *NMR Profiles* with micrometric resolution [26] and a maximum depth of the order of centimeters.

In this thesis, the MOUSE was controlled by a KEAII spectrometer. The KEAII is a complete NMR digital spectrometer suitable for performing a wide variety of NMR

experiments. It consists of many mules depicted in Figure 3.2, all powered from a 24 DC input. It is connected to the PC via USB interface and it is managed by the software.

3.1.2 Electromagnet Jeol

The apparatus located in the NMR laboratory of the Physics and Astronomy Department of the University of Bologna, is an in-house relaxometer based on a C60 H-L electromagnet controlled by the PC-NMR portable console (Stelar). Measurements reported in this thesis were performed at a frequency of 20.15 MHz for ^{1}H nuclei corresponding to a $B_0 = 0.473$ T. The coil has a cylindrical shape and it is located between polar expansion of the magnet where the field has the maximum homogeneity. The sensitive volume has a diameter d = 8 mm and a thickness l = 5 mm.
The acquisition is performed by the software AcqStelarNMR/FFC developed by Stelar.

3.1.3 Artoscan Tomograph

The Artoscan (Esaote S.p.A., Genova, Italy) is a tomograph characterized by a 0.2 T permanent magnet, operating at 8 MHz for ^{1}H nuclei. An important feature is the dimension of the magnet bore that allows to analyze samples of sizes up to 10 cm. The high homogeneity of the magnetic field and the possibility to use coil with different sizes make this instrument useful also for NMR relaxometry studies.

Figure 3.3: MRI apparatus based on the Artoscan Tomograph

3.1.4 Halbach Magnet: Benchtop MRI tomograph

The Benchtop MRI Tomograph is based on a cylindrical Halbach magnet characterized by a large sensitive volume in a highly homogeneous static magnetic field B0 = 0.6T, perpendicular to the cylinder axis. The magnet is composed by several individual block of permanent magnets aligned according to the geometry depicted in schematic of Figure 3.4a.

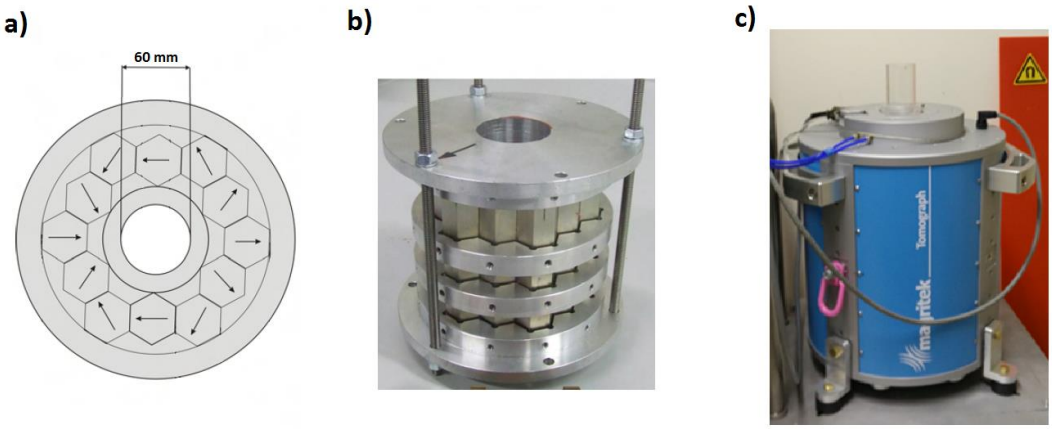

Figure 3.4: a) Sketch of magnet geometry. b) Magnet. c) Tomograph

The cylindrical coil is placed inside the magnet with the axis parallel to the magnet axis. The diameter of the coil is 60 mm and the height of the region in the homogeneous B0 is h = 60 mm. The instrument is designed for MRI analyses of medium-size samples, but I used this instrument for 2D-NMR relaxometry analysis. A KEA II spectrometer connected to a Personal Computer was used for piloting the experiment. The Benchtop MRI Tomograph is located in the NMR laboratory of Agrosphere Department of the Research Centre of Juelich, Germany. Moreover, in the same research Centre, I performed magnetic resonance imaging experiments on Varian tomograph based on a 1.5 T superconducting magnet suitable for analysis of large sample (i.e in-vivo study of trees).

3.2 Pulse sequences

In this subchapter, NMR pulse sequences are described. In particular, following descriptions are referred to pulse sequences dedicated to single-sided instruments and executed by the KEAII spectrometer.

MRI experiments in this thesis were performed by the use of a basic Spin Echo Multi-Slice sequence and no further specifications about imaging experiments are described in the following section.

3.2.1 One-Dimensional NMR Pulse Sequences

3.2.1.1 CPMG – Transverse Relaxation Time

One of the most frequently used RF sequence for characterizing the transverse relaxation time T_2 is the CPMG pulse sequence [27], [28]. A sketch of the sequence is presented in the Figure 3.5.

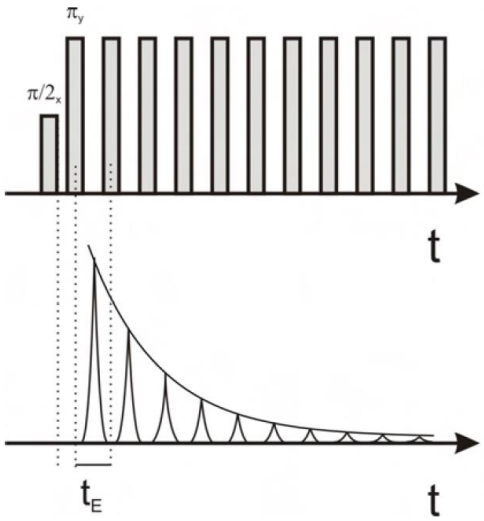

Figure 3.5: Sketch of the CPMG pulse sequence.

It consists of an initial π/2 pulse followed by a train of π pulses. The time interval between two π pulses is called t_e, echo time. The π pulse refocuses the magnetization dephasing due to B_0 inhomogeneity and it forms an echo of the signal at the measuring time $t = 2\ t_e$.

Through the transmission of a train of consecutive π pulses, it is possible to acquire the signal of the CPMG echo train governed by the T_2 relaxation process **Eq. 28**.

$$M(t) = M_0\, e^{-\frac{t}{T_2}} \qquad \text{Eq. 28}$$

where $t = n\tau$ with $n = 1, 2, 3, \ldots$.

3.2.1.2 Saturation Recovery – Longitudinal Relaxation Time

For instruments based on inhomogeneous magnetic fields, pulse sequences designed to measure the longitudinal relaxation time T_1 generally consist of three main parts. The first is a preparation stage, during which one or more radiofrequency pulses move the longitudinal magnetization away from its equilibrium state. The second is called free evolution period because the magnetization return in the equilibrium state through a relaxation process. The last is a detection period, in which the longitudinal magnetization is converted, by a π/2 pulse, into a transverse magnetization, in order to measure the system state achieved during the previous stage.

The most used sequences for determining T1 are the Inversion Recovery (IR) and Saturation Recovery (SR). In this thesis, measurements of the longitudinal relaxation time were performed by Jeol C60 H-L and Artoscan, using an IR sequence and by MOUSE, using a SR sequence. A sketch of the SR executed by NMR MOUSE is shown in Figure 3.6.

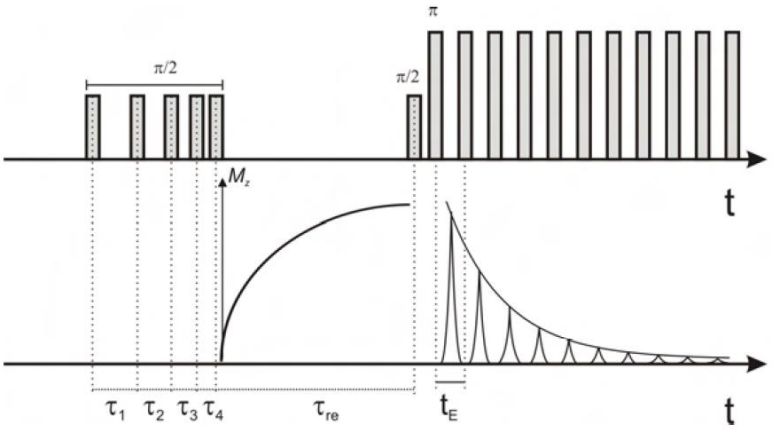

Figure 3.6 Scheme of the Saturation Recovery pulse sequence.

The sequence depicted in the figure above is composed by a saturation recovery (encoding sequence) and a CPMG (detecting sequence). Indeed, the first stage consists in an application of a train of π/2 pulses, in order to pre-saturate the transverse magnetization. In the second period, during a free evolution time interval τ, the longitudinal magnetization grows from zero to its maximum value M_0 through an exponential time dependence described by the equation:

$$M(\tau) = M_0\left(1 - e^{-\frac{\tau}{T_1}}\right) \qquad Eq.\ 29$$

After another π/2 pulse that rotates the longitudinal magnetization into the XY plane, a CPMG sequence is executed for the signal detection. Once the signal is acquired, the entire sequence is repeated varying values of the free evolution period τ in order to sampling the build-up curve of the longitudinal magnetization. For obtaining an

appropriate sampling τ is varied logarithmically because the acquired process is expected to be an exponential.

Extrapolating for t = 0 the magnetization value of acquired CPMGs it is possible to follow the trend of the longitudinal magnetization $M(\tau)$ and to estimate the longitudinal relaxation times distribution through Laplace Inversion of data.

3.2.1.3 Stimulated Echo – Diffusion coefficient

The stimulated echo sequence is often used to investigate the diffusion coefficient of molecular fluids [29]. In order to exploit long diffusion times respect to Spin-Echo based sequences, during the diffusion period the magnetization is stored in z-direction where it decays due to T_1 relaxation process. The sketch of the sequence is depicted in Figure 3.7.

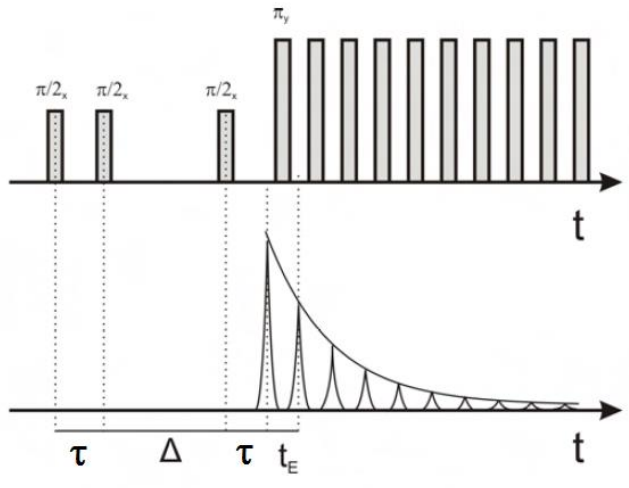

Figure 3.7: Sketch of the Stimulated Echo sequence.

The first pulse is a $\pi/2$. After a time τ, a second $\pi/2_x$ is applied with the consequent rotation of the y-component of magnetization into the z-axis, in which the relaxation occurs according the time constant T_1. This period is allowed to evolve for a time Δ and then the stored longitudinal magnetization is converted into transverse magnetization by the use of another $\pi/2_x$ pulse. In the last stage, the signal is acquired by a CPMG sequence.
The signal attenuation caused by the diffusion process occurred during the evolution time interval Δ result to be:

$$ln\left(\frac{S}{S_0}\right) = -\gamma^2 G^2 \tau^2 D\left(\Delta + \frac{2}{3}\tau\right) \qquad Eq.\ 30$$

G is the intensity of the field gradient, D the diffusion coefficient, γ the gyromagnetic ratio and τ is the encoding time.
In the case of molecular fluids filled porous media, the Stimulated Echo sequence makes possible the evaluation of the SVR of the confining geometry [30]. Indeed, varying the value of Δ parameter, the behavior of the diffusion coefficient $D(\Delta)$ can be analyzed in order to obtain an estimation of the SVR according to the Eq. 4 described in the Subchapter 2.2.

3.2.2 Two-Dimensional NMR Pulse Sequences

3.2.2.1 Saturation Recovery – CPMG: T_1-T_2 Correlation

The analysis of T_1-T_2 correlation function was performed by the MOUSE PM25 on porous media filled with water. The pulse sequence used for this study is described in

subsection 3.2.1.2 with an important difference. In the sequence previously described, the CPMG is executed only for extrapolating a value of the magnetization, while, in this case, the sequence is entirely stored for each value of τ. In this way, by repeating the SR-CPMG varying τ for *m* times, and acquiring signals through the use of *n* echoes of the CPMG sequence, a data matrix Y of sizes *m* x *n* is stored.

For the evaluation of the T_1-T_2 correlation map, the data matrix is processed according to the method described in the subchapter 2.4 by a 2D-ILT. In this case, kernels related to relaxation processes are k_1 and k_2 with

$$k_1 = \left(1 - e^{-\frac{\tau_1}{T_1}}\right) \qquad and \qquad k_2 = e^{-\frac{\tau_2}{T_2}}.$$

An example of a data matrix Y and the corresponding two-dimensional Laplace transformation is depicted in Figure 3.8.

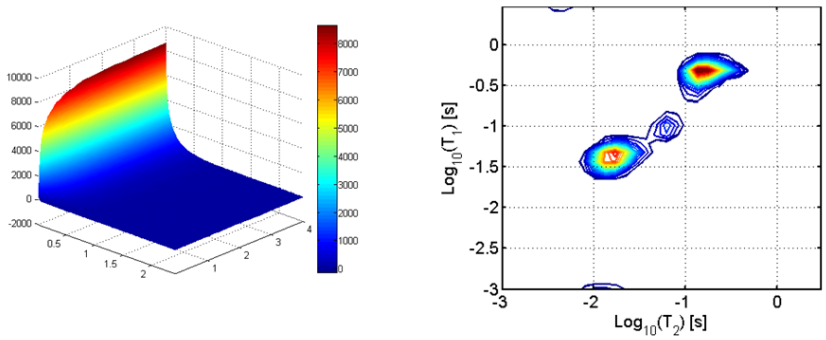

Figure 3.8: Example of T_1-T_2 data matrix Y on the left, and the resulting map on the right.

3.2.2.2 CPMG – CPMG: T_2-T_2 Relaxation-Exchange

The pulse sequence performed for the study of relaxation-exchange correlation function [31] is sketched in Figure 3.9.

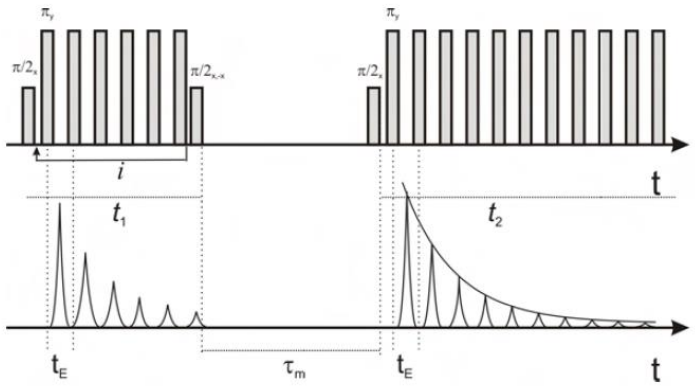

Figure 3.9: Sketch of the CPMG-CPMG sequence.

Three main periods are distinguished. During the first period, a CPMG is performed for encoding the first dimension of T_2 relaxation process. At the end of the first stage, a $\pi/2$ pulse rotates the magnetization along the longitudinal axis and a time interval τ_m (mixing time) is waited. During this time the magnetization evolution follows the T_1 process. At the end of the second period, another CPMG sequence is applied in order to detect the signal. The CPMG-CPMG sequence is repeated for *m* times, each time increasing the number of echoes of the first CPMG and acquiring the signal by *n* echoes of the second CPMG. When the experiment is finished, a data matrix Y of sizes *m* x *n* is acquired. For the evaluation of the T_2-T_2 correlation map, the data matrix is processed according the method described in the subchapter 2.4 by a 2D-ILT. In this case, kernels related to relaxation processes are k_1 and k_2 with

$$k_1 = e^{-\frac{\tau_1}{T_2}} \qquad and \qquad k_2 = e^{-\frac{\tau_2}{T_2}}.$$

In general, the exchange process is detectable through the map by the presence of off-diagonal peaks for values of τ_m longer than the shorter T_1 relaxation class. Usually these peaks are symmetric respect to the principal diagonal and their coordinates are representative of relaxation rates of different classes of pores. But the interpretation of 2D exchange-relaxation maps is not trivial [32]. The reason is in the interaction between exchange and relaxation processes during different periods of the pulse sequence. Indeed, the relaxation, probed during the encoding periods, implies that exchange can never be restricted to the mixing period and must also be considered during the encoding periods. As a consequence, the two-dimensional relaxation exchange map cannot be interpreted as pure exchange maps but as exchange probability densities. Moreover, due to this behavior, relaxation exchange maps are often non symmetric and peak positions are shifted from the cross coordinates of the apparent relaxation rates identified on the diagonal.

3.2.2.3 Stimulated Echo - CPMG: D-T_2 Correlation

The diffusion coefficient D of a hydrogenous fluid can be mapped in correlation with the T2 relaxation process. The specific sequence executed by NMR MOUSE PM25 is a Stimulated Echo – CPMG [33], [34]. As in the case of SR-CPMG sequence, the sequence used for this study is the same of the one describe in the one-dimensional experiment of Stimulated Echo sequence, Figure 3.7, subsection 3.2.1.3. Also in this situation the CPMG is acquired and *n* number of echoes are entirely stored. The combination STE-CPMG is repeated for *m* times, varying the encoding parameter τ. In this way, at the end of the experiment the data matrix Y of sizes m x n is stored for a fixed value of Δ. For the

evaluation of the D-T_2 exchange-relaxation map, the data matrix is processed according the method described in the subchapter 2.4 by a 2D-ILT. In this case, kernels related to diffusion and relaxation processes are k_1 and k_2 with

$$k_1 = e^{-\gamma^2 G^2 \tau_1^2 D(\Delta + \frac{2}{3}\tau_1)} \qquad and \qquad k_2 = e^{-\frac{\tau_2}{T_2}}.$$

Correlation D-T2 maps. In particular, as the value of parameter Δ, time leaved for the diffusion process, increases, much more time is given to spins for moving. In a restricted geometry, like inside a porous medium, the value of the diffusion coefficient is attenuated, due to SVR of the confining pore, as a function of the diffusion time Δ. Thus, increasing the value of Δ and crossing the information about the transverse relaxation process to the one about the diffusion phenomenon, it possible to distinguish different classes of pores and follow their own diffusion behaviors.

4 ADVANCED APPLICATIONS: ENVIRONMENTAL SUSTAINABILITY

4.1 Cultural Heritage

The preservation of historical buildings and outdoor cultural assets is a necessity for the humankind because the artworks are the testimony of our past, as well as an economic resource for the present and future times. The main causes of degradation of stones, the more important porous materials for these artifacts, are linked to chemical-physical processes that influence the ingress and diffusion of water (liquid or vapour) into the porous structure. Water, in fact, in the condensed phase dissolves CO_2 and pollutants from the atmosphere, causing acidic corrosion of the stone or the binder, and it is responsible of internal mechanical stresses caused by freezing-thawing cycles or salt crystallization [35]–[38].

In this NMR study, I tested the efficiency of protectives and consolidants applied for preserving carbonate stone material, of interest to Cultural Heritage, from the damage caused by atmospheric agents.

4.1.1 Protective compounds

The use of hydrophobic compounds, typically synthetic polymers, is a common practice to protect surfaces from water [39], [40]. However, it has been demonstrated that the efficiency and durability of the treatments depend on the characteristics of the compounds used, on the treatment procedure and on the chemical-mineralogical nature of the substrate. In particular, for an effective preservation of the substrate [40], the protective agent must have a uniform distribution, good penetration into the porous structure, and low propensity to pore blockage. Last but not least, the protective compound must be soluble in benign solvent for operators and environment.

Among the protective agents used to protect porous materials, perfluoropolyethers have many of the properties required for an ideal protection, such as high stability, water repellency and low surface tension. Unfortunately, these compounds are soluble only in chlorofluorocarbons (CFC) and in supercritical CO_2, therefore their use as protective agents for historical stone artifacts has been abandoned since 1995.

Therefore, this work was focused on the preparation of a new low average molecular weight protective agent containing short pendant perfluoropolyether segments linked to an oligo(succinamide) chain (SC2-PFPE) in order to realize a compound characterized by the protective action of the perfluoropolyethers and the solubility in environmental friendly solvents. The product was synthetized and the treatments were performed by M. Camaiti (CNR-IGG, Florence).

4.1.1.1 Materials and methods

Samples (5x5x2 cm^3) of Lecce stone, a biocalcarenite with total porosity P=46-48%, porosity accessible to water PH_2O= 39%, were used to test the performances of the

protective treatments. The pore-space of this stone is macroscopically very homogeneous but there is a substantial range of pore and pore-channel sizes: Mercury Injection Porosimetry gives a range from 0.01 μm to a few micrometers, with a sharp peak at just over 2 μm.[8]

The hydrophobic treatments were performed on only one 5x5 cm^2 surface of the prismatic stone samples using SC2-PFPE and a commercial fluoroelastomer (N215) as a reference. SC2-PFPE is an oligo(ethylensuccinamide) containing low molecular pendant perfluoropolyether segments. The compound was applied both as 0.5% (w/w) solution in a mixture of 2-propanol:H_2O (70:30, w/w), and as 1% (w/w) suspension in a mixture of 2-propanol:H_2O (70:30, w/w). N215 was applied as 1% (w/w) ethyl acetate solution. For all products the amount of solution/suspension to be applied was calculated considering a final theoretical amount of active compound on the stone surface of 10 g/m^2. The solution/suspension was deposed on the stone sample by pipette. The solvent was evaporated at laboratory conditions and then the stone specimens were dried in desiccator to determine the mass of active product actually applied before subjecting them to the tests for performance evaluations. Three samples for each treatment were prepared. All of them were used for the water capillary absorption test and then two were used for the vapor permeability test and the third for the photo-stability measurements. One of the two specimens used for the evaluation of vapor permeability was later used for the MRI analysis.

MRI images were collected using Artoscan (Esaote S.p.A., Genova, Italia), a tomograph based on a 0.2 T permanent magnet, operating at 8 MHz for ^1H nuclei. Multi-slice Spin-echo sequences were used to obtain at the same time a number of adjacent axial sections on each sample sufficient to cover all the sample (thickness of each slice = 5 mm, gap

between slices = 1 mm, pixel size = 0.78 x 0.78 mm^2, Repetition Time (TR) = 900 ms, Echo Time (TE) = 10 ms, number (N) of Scans = 8). Bright regions in MRI images reveals the presence of water (the signal is due to the ^1H nuclei magnetization). The signal in each pixel is proportional to the water amount in the corresponding voxel only if the nuclear magnetization is allowed to reach the equilibrium after each acquisition sequence. In porous media, wide distributions of longitudinal and transverse relaxation times T_1 and T_2, due to wide distributions of pore sizes, are observed. In order to allow all components to reach the equilibrium, it is necessary to have an echo time TE much shorter than the shortest T_2 component inside the sample and a repetition time TR much longer than the longest T_1 component in the sample. These conditions conflict with instrumental limitations (minimum TE is 10 ms) and measurement duration, which is proportional to TR. MRI images were taken at increasing intervals of time during capillary water absorption, from one hour up to a week. Images were analyzed by an in-house software in order to quantify the water signal (in arbitrary units) inside the samples, in a scale that was the same for all the samples. From each slice, the algorithm also created a signal profile along the shortest side of the sample by the sum, for each row of the image, of the values of all the pixels. In order to characterize the spatial distribution of the water in the stone, the three-dimensional view of the sample was reconstructed starting from the two-dimensional slices, by implementing an algorithm under the Enthought Canopy environment, a Python academic free distribution for scientific and analytic computing.
MOUSE PM 25 was used in order to realize a 1D diffusometry study and 2D correlation maps. All the following analyses were executed with the sensitive volume centered About diffusometry, the Stimulated Echo sequence was applied with Pulse Length = 12 μs, TR = 5 s, TE = 80 μs, number of echoes = 512, τ varying from 0.08 ms to 0.4 ms with 32

steps and for each experiment the mixing time Δ was varied and it assumed the following values (4, 12, 50, 100, 150, 200 and 400) ms. In this way, according to the Eq. 30, the value of D(Δ) was calculate, for each Δ, and the SVR was evaluated following the Eq. 6. 2D NMR was performed by STE-CPMG and SR-CPMG pulse sequences, in order to study correlation functions D-T2 and T_1-T_2 and, respectively. The STE-CPMG was set up with the same parameters of 1D STE with the exception of a higher number of echoes in the CPMG sequence (4000 echoes) in order to sample the entire relaxation signal. The SR-CPMG was performed with the following parameters: the SR was sampled with 128 points logarithmically spaced from a value of 0.1 ms to a value of 6 s, while the CPMG was set with the same parameters used in the STE-CPMG. The 2D inversion was performed by an algorithm based on the work of Venkataramanan [41].

4.1.1.2 Results and discussion

MRI is a method, not conventional for these kind of investigations, that allows the visualization of liquid water inside a porous material and allows to test the hypothesis on the different penetration depth and distribution of the products in the different treatments. The evaluation of the protective efficacy by UNI-EN 15801-2010 method [42] is obtained by water absorption through the treated face. On the contrary, the MRI analyses were performed with water absorption through both the treated and the untreated face, giving clear and reliable results. Indeed, in the extreme condition of the hydrophobic product concentrated on the treated surface, the absorption through the treated face would produce dark images (typically black), because the hydrophobic compound would block the ingress of liquid water. On the contrary, the absorption carried out through the untreated face would determine bright images, similar to those of the not treated samples. The

hydrophobic treatments performed in this work never gave rise to the limit condition exposed above, and the different behavior and properties of these stone protective agents and treatments were clearly demonstrated through the comparison of the MRI images acquired after water absorption through both the treated and the untreated face.
Figure 4.1 reports the images of an internal slice of the specimens during the kinetics of water absorption through the treated surface.

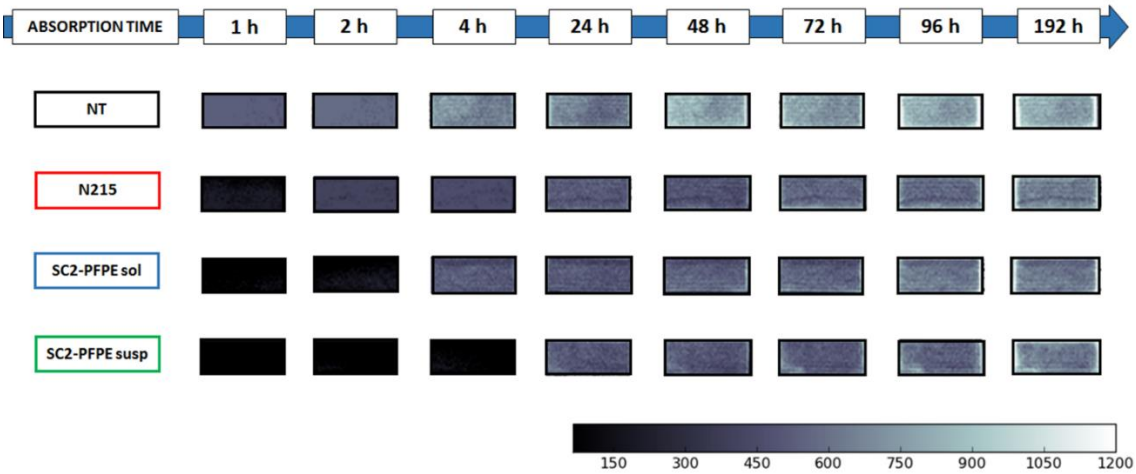

Figure 4.1: MRI images of an internal section of the samples of Lecce stone, over time of water absorption from the treated face. NT is the untreated sample. N215 is the sample treated with fluoroelastomer, SC2-PFPEsol and SC2-PFPEsusp are the samples treated with SC2-PFPE in solution and in suspension, respectively. The LUT represents the signal intensity in arbitrary units.

The images of the samples treated with the partially fluorinated oligoammide (SC2-PFPE) show a more prolonged resistance to water uptake than that treated with the fluoroelastomer (N215). In fact, the images corresponding to the samples treated with SC2-PFPEsol and SC2-PFPEsusp appear dark (almost black) up to 2h and 4h of water

absorption, respectively, while those of the sample treated with N215 show slow but progressive ingress of water already at 1h of absorption. After longer absorption times (up to 192 h – 8 days) water can penetrate and is distributed in the entire sample for all the treatments, confirming the substantial absence of closed pores, in accordance with the high residual permeability to vapor (data not reported). By comparing the gray levels of the images with the look up table (LUT) the final amount of water absorbed appears less in the treated samples than in the untreated one. Quantitative data on the mass of water absorbed (Figure 4.2) confirm the information obtained by the images: the untreated sample absorbs more water (about 15-20%), and faster, than the treated samples.

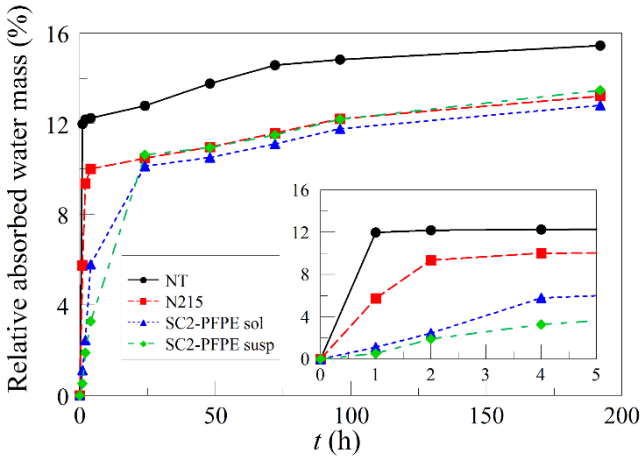

Figure 4.2: Water mass per dry mass (%) absorbed from the treated face of the samples of Figure 4.1 as a function of time.

The higher amount of water absorbed by the untreated sample cannot be due to a different water uptake ability of this sample (typically ascribed to different porosity and pore sizes) in respect to the other three samples, but only to the presence of the protective agent inside

the pore space. In fact, in the water capillary test carried out on the same samples before the treatment, the same untreated specimen absorbed less amount of water than the other samples (data not reported).

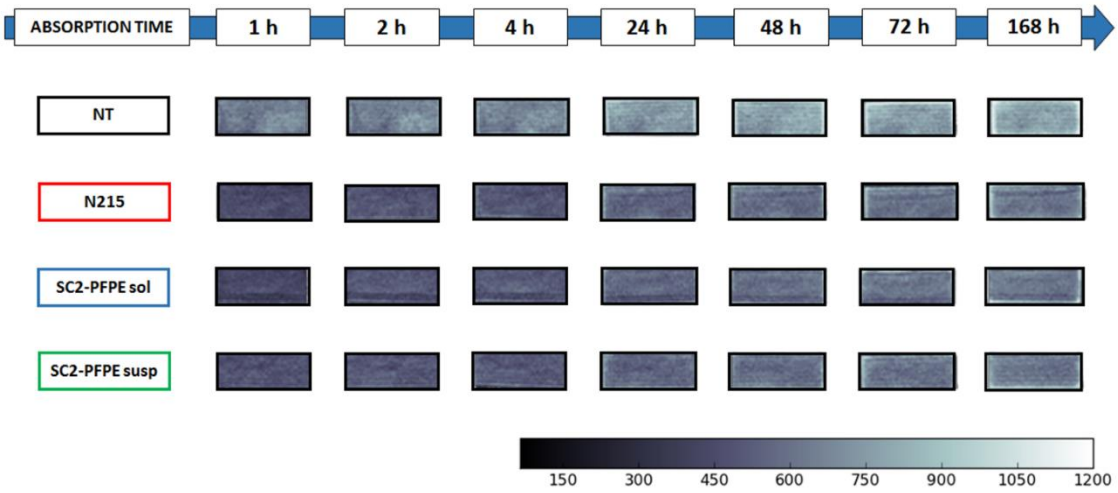

Figure 4.3: MRI images of an internal section of the same samples of Lecce stone in Figure 4.2, over time of water absorption from the untreated face.

The images of the kinetics of water absorption through the untreated face (Figure 4.8) show slower and less water absorption than the untreated one, both at short (1 h) and long times (168 h - 7 days) of absorption.

In this case, all the hydrophobic treatments give the same trend in terms of mass of water (Figure 4.2), also for short absorption times (0-5 h), but the images of samples treated with N215 and SC2-PFPEsol show a non-uniform distribution of water. In the case of N215 a darker region at about 5 mm from the treated surface, well visible at long

absorption times (≥ 24h) (Figure 4.1 and Figure 4.3), indicates that the polymer is concentrated near the treated face. On the contrary, in the case of SC2-PFPEsol a darker region is visible at about 5 mm from the untreated face.

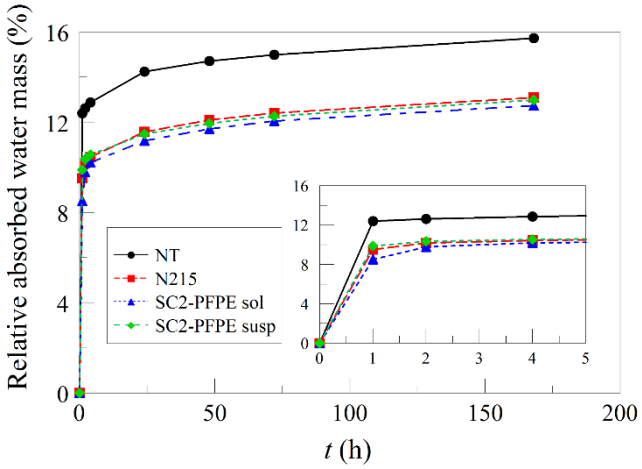

Figure 4.4: Water mass per dry mass (%) absorbed from the untreated face of the samples of Fig.4-1 as a function of time.

This region is already visible after 1h of water absorption if the test is performed through the untreated face (Figure 4.3), and after longer times (4h) when it is carried out through the treated face (Figure 4.1). This effect is observed in the entire sample, not only in the section shown in Figure 4.1 and Figure 4.3. Figure 4.5 is a three-dimensional view of this specimen in false colors, reconstructed from all the adjacent slices, after 4 hours of water absorption through the untreated face. This behavior is justified with a high propensity of SC2-PFPEsol to penetrate inside the porous medium, with an accumulation of the product at the face opposite to the treated one due to the limited thickness of the specimen (2 cm). Since the initial kinetics of water absorption through the untreated face

is similar for all the treatments (inset of Figure 4.4), the accumulated protective agent does not seem to substantially reduce the water ingress in this sample.

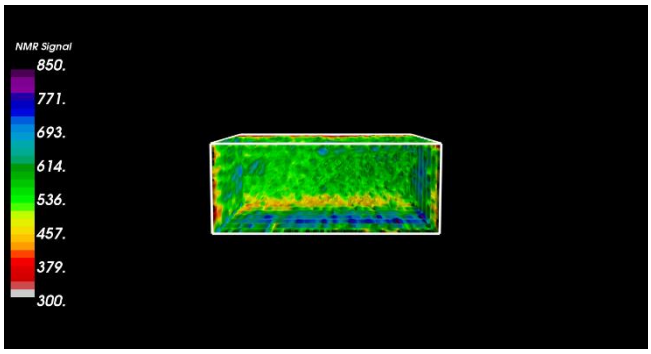

Figure 4.5: Three-dimensional reconstructed MRI image of the Lecce stone sample treated with SC2-PFPEsol after 4 hours of water absorption through the untreated face.

As known, the velocity of water ingress is governed by the smallest pores, the results shown above suggest that SC2-PFPEsol is mainly distributed in medium-large size pores. The high hydrophobicity of SC2-PFPE, as suggested by the low wettability of the treated surface, is responsible for lowering the concentration of liquid water in the region of the protective agent accumulation, as well as for reducing the vapor condensation. This last consideration justifies the lower values of the vapor permeability observed for SC2-PFPEsol treatment in respect to the other two treatments (data not reported).

Finally, the different hydrophobic effect given by the three treatments is well summarized in Figure 4.6, where for each sample an internal section is shown along with the corresponding profile of water absorbed after 4 hours of capillary absorption through both the treated and the untreated face.

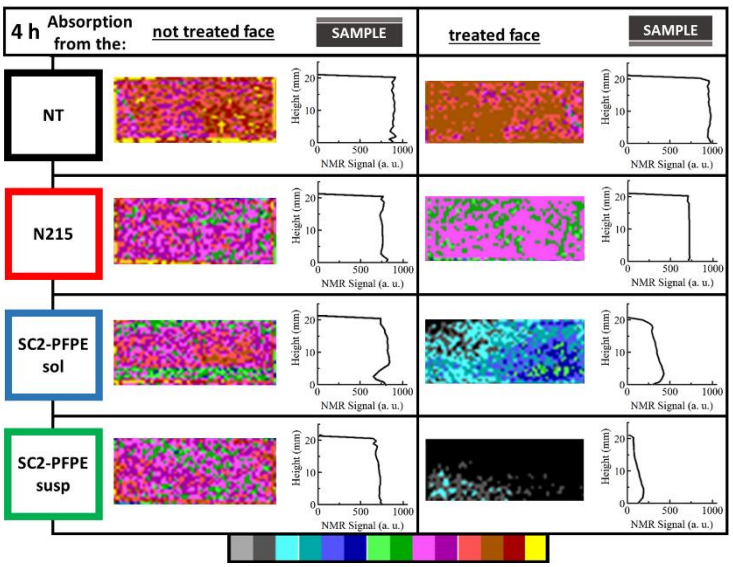

Figure 4.6: MRI images and corresponding water content profiles of the internal slices of the same samples of Lecce stone reported in Figs. 4-1 and 4-3, for water absorption from the untreated (left) and the treated (right) face, after 4 h of water capillary absorption. The LUT colors from grey to yellow show increasing signal values.

In order to obtain an in-depth study about limestone samples, the apparent self-diffusion coefficient behavior was investigated varying Δ parameter. For each sample seven different Stimulated Echo experiments were performed (Δ = 4, 12, 50, 100, 150, 200, 400) ms. Thus, from each Stimulated Echo experiments the value of D(Δ) was calculated, according to the Eq. 29. For porous media saturated with fluids characterized by spherical pores interconnected, the behavior of diffusion coefficient D(Δ) follows the Eq. 6. Through this relationship, it was possible to estimate the average value of the apparent self-diffusion coefficient as a function of parameter Δ. The diffusional coefficients as function of the observation time Δ are shown in Figure 4.7.

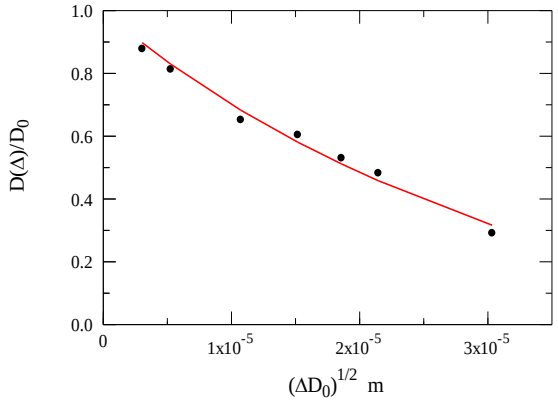

Figure 4.7: Diffusional coefficient as function of Δ. Untreated sample.

Data, black points, were fitted by the Eq. 6, and the result is plotted as a red line. The initial slope of the trend is depended on the surface to volume ratio of the confining geometry. Thus, assuming pores as spheres, the average pore radius was estimated. Results of this procedure are shown in Table 4.1.

Sample	S/V	R_{avg} (μm)
SC2-PFPE sol	2,0E+05	15
SC2-PFPEsusp	1,4E+05	21
N215	3,1E+05	10
Reference	8,3E+04	36

Table 4.1: SVR and average pore size estimated for Lecce stone samples.

All the treated samples exhibit higher surface to volume ratios than the reference. This effect can be explained by the action of hydrophobic treatment that creates a thin layer of the product inducing a reduction of the average pore sizes.

Last measurements on Lecce stone samples were performed by the use of SR-CPMG and STE-CPMG pulse sequences in order to obtain 2D correlation maps T_1-T_2 and D-T_2 respectively.

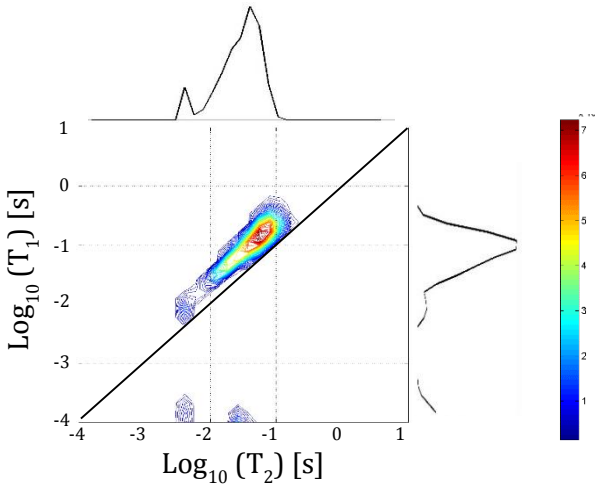

Figure 4.8: Reference sample. T_1-T_2 map on the left and D-T_2 map for Δ=4 ms on the right.

The T_1-T_2 map of the reference sample is depicted in Figure 4.8. No significant differences were noted among maps of treated samples, thus only the maps related to the reference was reported. The shape of the 2D distribution is closely parallel to the line for $T_1 = T_2$, meaning that all the water molecules in this rock have an identical T_1/T_2 ratio and T_1 times are always higher than the correlated T_2 times. This behavior is consistent with the interpretation, presented in the subsection 2.1, in which the relaxation process in porous media is caused by a single surface relaxation mechanism and the distribution of T_1 and T_2 is due to the variation of local surface-to-volume ratio, or pore sizes. These results are compatible with the those reported by [21] for Indiana limestone.

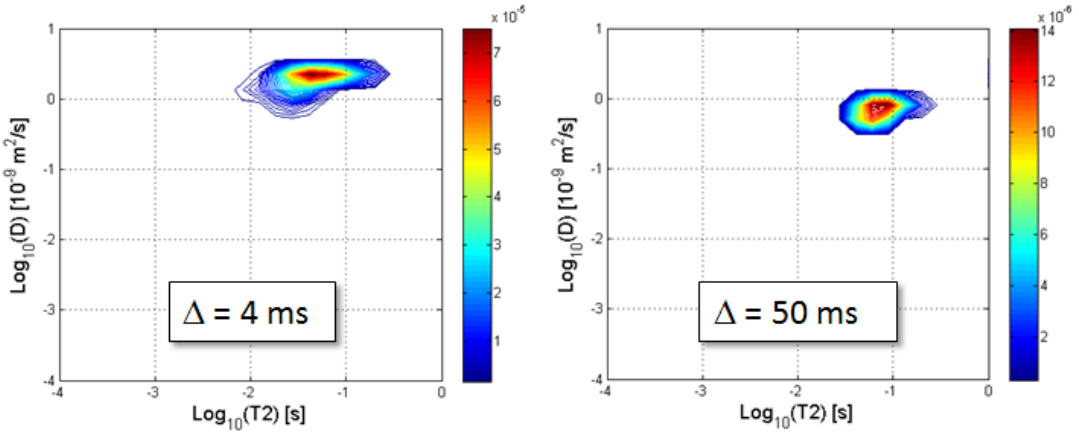

Figure 4.9: D-T_2 maps of reference sample for mixing time values Δ = 4 ms and 50 ms.

Figure 4.9 depicts an example of D-T_2 maps obtained for the reference with Δ = 4 ms and 50 ms. For a mixing time Δ = 4 ms, the map shows that the component with shortest T_2 times (between 1 ms and 10 ms, Figure 4.8) disappears while the remaining component exhibits a diffusion coefficient similar to bulk water. This effect indicates that the magnetization of the water in small pores (short transverse relaxation times), is totally decayed because the diffusion motion has accelerated the surface relaxation process, while for water in large pores, the effect of the diffusion has not influenced the effective relaxation rate (the measured diffusion coefficient for this component is similar to the one of bulk water). The map with Δ = 50 ms shows an attenuation of the diffusion coefficient respect to the bulk value and the enhancement of the effect described for Δ = 4 ms. Increasing Δ, the attenuation of the signal-to-noise ratio made not possible a punctual analysis of the resulting maps. A more efficient measurement procedure will be applied in order to overcome this issue.

4.1.1.3 Conclusions

The new oligo(ethylensuccinamide) containing low molecular pendant perfluoropolyether segments, easily synthesized by two-step poly-condensation reactions, shows suitable characteristics to be used as protective agent in porous materials, like calcareous stones. Its low solubility in alcohols or hydro-alcoholic solvents makes possible its application on the surfaces without any environmental negative impact. The presence of low molecular pendant perfluoropolyether segments guarantees good stability to UV irradiation (data not shown), and, at the same time, greatly improves the water repellence in respect to others fluorinated compounds (i.e. fluoroelastomer). The high hydrophobic properties are due to the orientation of the fluorinated segments at the interface air/stone surface, while the not fluorinated amidic groups of the oligo(ethylensuccinamide) interact, via hydrogen bonds, with the stone giving a good permanence of the product on the surface also after ageing (UV irradiation and wet-dry cycles (data not shown)N215 slightly reduces the water uptake but the better performance of SC2-PFPE due to the influence of the hydrophobic perfluoropolyether pendant segments is evident, in accordance with their ability to arrange at the interface substrate/air in consequence of the strong segregation due to their low surface free energy [43], [44].

This study has also confirmed that MRI is an excellent technique for evaluating the performances of hydrophobic compounds and, in particular, of these fluorinated products. Indeed, traditional methods cannot give information on the spatial distribution of the product on the surface of the internal surfaces of the pore space, but allow to formulate hypotheses that only MRI can validate. The images give also further information about the distribution of the products (the accumulation of the fluoroelastomer at the treated

surface, and the accumulation of SC2-PFPEsol at the untreated face of the sample) that traditional tests cannot even suspect.

4.1.2 Consolidative compounds

In this paragraph, results of the application of different NMR techniques for the performance evaluation of consolidants are disclosed.

4.1.2.1 Materials and methods

Maastricht stone is the material used in this analysis. It is a calcarenite characterized by a porosity P=48-50% and it was chosen because the high porosity well simulates a high-deteriorate carbonate rock. The study investigates the efficiency of commonly used consolidants for carbonate stone material like the ethyl silicate ESTEL 1000, distributed by CTS s.r.l., and nano-silica particles. These consolidants are hydrophilic, so they tend to absorb water. Unfortunately, water is one of the main agent [45] of degradation of stone materials used for architectural constructions. For this reason, we tried to exploit the hydrophobic behavior of a common protective compound, fluoroelastomer N215, to reduce the hydrophilic property of common consolidants. A new compound was synthetized mixing the nano-silica and the fluoroelastomer. Figure 4.10 summarizes the products used.

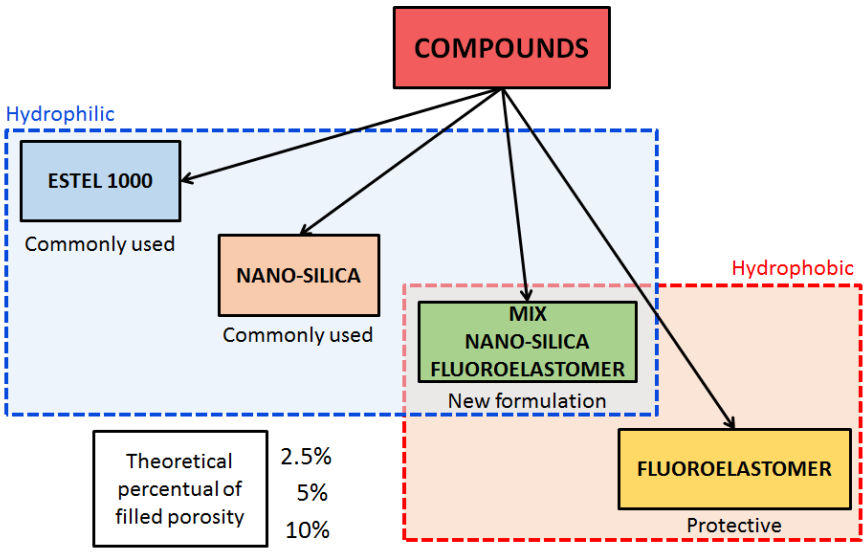

Figure 4.10: Schematic of consolidants applied to Maastricht stone.

The application of consolidants was executed by a pipette covering the entire surface of one of the largest face of the stone sample, this face is called treated face. Syntheses and treatments were

Performed by Mara Camaiti (CNR-IGG, Florence). The Maastricht stone was treated with different quantities of products. In particular, the amounts of product applied for treatments were calculate in order to fill specific percentages of the porosity of the stone 2.5%, 5% and 10%. In the table below applied quantities are listed. The application of the products was similar to the procedure used in subsection 4.1.1.1.

Compound	Sample n°	Specifications	Theoretical Filled Porosity (%)	Theoretical amount (g)
Not treated (reference)	35	-	-	-
	36	-	-	-
	55	-	-	-
Ethyl silicate ESTEL 1000	40	ESTEL 1000, applied 3.2 ml	2.5	0.754
	38	ESTEL 1000, applied 6.4 ml	5	1.508
	39	ESTEL 1000, applied 12.8 ml	10	3.016
	44	ESTEL 1000, applied 12.8 ml	10	3.016
	45	ESTEL 1000, applied 12.8 ml	10	3.016
Nano-Silica	42	Nano-silica 10%, applied 7.54 ml	2.5	0.754
	33	Nano-silica 10%, applied 10.4 ml	3.4	1.04
	41	Nano-silica 10%, applied 15.08 ml	5	1.508
Fluoroelastomer N215	43	N215 at 7% in acetone, applied 15.64 ml	2.5	0.92
	37	N215 at 7% in acetone, applied 33.2 ml	5	1.84
Mix Nano-Silica + N215	52	Mix N215 at 7% in acetone + nano-silica 5%, applied 21.5 ml	2.5	0.812
	50	Mix N215 at 3.5% in acetone + nano-silica 10%, applied 17.0 ml + 6 ml acetone in three times	4.1	1.338

Table 4.2: Details about the consolidating treatments.

The experiment consisted in two main steps.

1) *Controlled Relative Humidity (RH)*: the water vapor absorbed by the stone was monitored under controlled conditions of RH. The determination of transverse relaxation

time behavior allows to quantify and understand the behavior of the water into the porous structure of the stone.

First of all, samples were left a couple of week inside a desiccator to reach the condition "dry". After this period, they were weighted by an electronic balance and sealed in custom-made glass boxes for preserving the dry state. Once the stone was sealed, the box was leant on the NMR probe MOUSE PM25 and analyzed by a CPMG pulse sequence with a Pulse Length = 12 µs, TR = 2.5 s, TE = 80 µs, number of echoes = 800 and 9000 Scans. The MOUSE was used in the configuration with 10 mm spacers inserted. The signal was acquired in a volume of sizes 25x25x0.3 mm^3 located in the middle of the sample, 10 mm from the treated face. The Inverse Laplace Transform was performed by the software UPENwin (University of Bologna) based on the algorithm UPEN [46], [47].

To control RH, a fully-saturated $NaCl+H_2O$ solution is used in a glovebox, assuring a constant RH of 75%. The temperature was stable ~ 25 °C. Samples were located into the glovebox for three days, the minimum time period tested to reach the saturation of water vapor. After this period samples were weighted, then they were sealed into the glass boxes and they were measured by the MOUSE using the same procedure used for the dry samples.

2) Full Saturation: Dry samples were weighted. Then they were saturated under vacuum (pressure reached inside the chamber Ps=1 mbar) with deionized water. After the process samples were weighted and promptly sealed into glass boxes, to avoid the alteration of the condition.

MRI images were collected using a tomograph (Varian) based on a 1.5 T superconductor magnet. Spin-echo Multi-slice sequences were used to obtain at the same time a number of adjacent axial sections with a FOV = 60x40 mm^2. The thickness size of each slice was

1 mm, the gap between slices 0.1 mm, the pixel size 0.23x0.16 mm^2, TR= 2.5 s, TE= 4 ms and the number of scans 4. Data were processed by the free-license software ImageJ in order to obtain a signal intensity profile. For the analysis, a rectangular ROI was taken around the shape of the sample section and the value of the calculated profile was averaged all over the slices.

MOUSE PM25 was used in order to collect proton density profiles of saturated samples. Stones were positioned on the flat coil of the device with the treated face oriented to the instrument. A CPMG sequence was used for estimating the proton density. Principal parameters of the sequence were: Pulse Length = 12 µs, TR = 5 s, TE = 80 µs, number of echoes = 2048, resolution = 300 µm and number of Scans = 32. In order to obtain the profile, the automated lift was set with a step size Stp = 300 µm for a total distance of 22.2 mm.

Two-dimensional NMR relaxometry measurements were collected by the Benchtop MRI Tomograph (Magritek) based on a 0.5 T Halbach magnet. T_2-T_2 relaxation-exchange experiment was performed by a CPMG-CPMG pulse sequence (Pulse Length = 44 µs, TR = 5 s, TE = 300 µs, number of echoes = 2800, number of Steps = 128 and number of Scans = 16) repeated varying the Mixing Time according to the following values: 0.5, 10, 50, 100, 150 ms. A software based on the algorithm of Venkataramanan [41] performed the two-dimensional Inverse Laplace Transform to the collected data matrix (2800x128) in order to realize a 64x64 map.

In the following subsections, the principal results are discussed.

4.1.2.2 Controlled Relative Humidity results and discussions

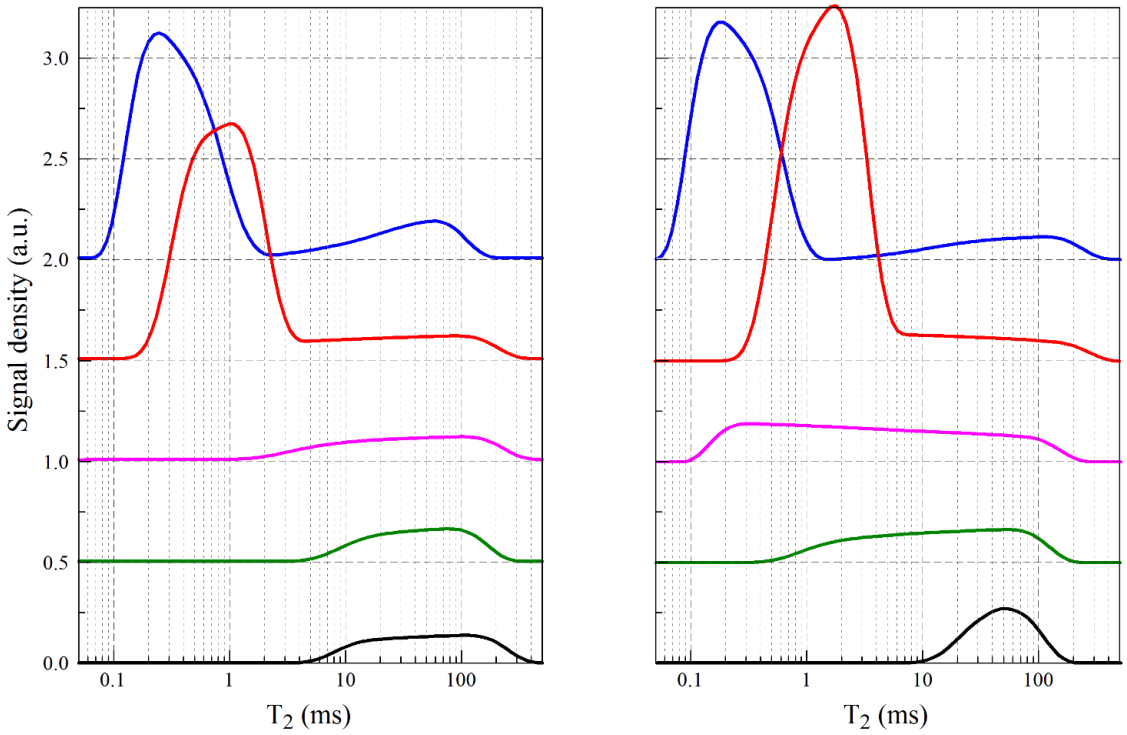

Figure 4.11: Distribution of transverse relaxation times for samples in the desiccator, on the left, and samples in the condition of RH=75%, on the right. Reference (black), new synthetized compound (green), nano-silica (pink), ethyl silicate (red) and fluoroelastomer (blue).

TREATMENT	Absorbed Water Vapor (mg)
REFERENCE	34
FLUOROELASTOMER	40
ESTEL 1000	126
NANO-SILICA	486
MIX	244

Table 4.3: Absorbed water (mg) computed as wet mass - dry mass for all the treatments.

The most relevant results obtained by the experiment under controlled RH conditions are showed in Figure 3.1 where transverse relaxation time distributions of samples treated with 5% of theoretical filled porosity are displayed for the condition of dry sample, desiccator, on the left and of wet sample, glovebox at 75% of RH, on the right. Sample treated with the nano-silica compound, green line, shows relaxation times similar to the reference for the sample in the desiccator and it shows a broadening of the relaxation curve with a shift to short times, up to ~1 ms.

The behavior of transverse relaxation times for the stones treated with ESTEL 1000 and the fluoroelastomer is different from the reference. In particular, most of the signal, characterized by a peak, comes from short relaxation times at ~ 0.1 – 1 ms, and it is proportional to the amount of applied product. This feature indicates the presence of water restricted in very small pores probably trapped inside the porous space during the treatment.

For the fluoroelastomer, there are no relevant differences in the relaxation curves of dry and wet conditions, confirming the results of the electronic balance that shows only a very small amount of water vapor absorbed by the stone in the RH condition, see Table 4.2. The ESTEL treated sample, according to weight showed in Table 4.2 absorbed a considerable quantity of water revealed by the increased area under the peak of the wet condition respect to the dry condition.

Green colored curves show the relaxation behavior of the sample treated with the new synthetized compound. The trend is intermediate between the nano-silica and the ESTEL1000 ones, confirming what was expected during the synthesis of this product. Furthermore, the electronic balance results show an intermediate amount of absorbed water between the ESTEL and the nano-silica, in agreement with the initial idea of trying to reduce the hydrophilic property of the silicate particles by the use of a fluoroelastomer. The experiment of monitoring samples in controlled RH conditions allowed us to study the behavior of stone samples treated with consolidants in conditions that well simulate the natural conditions of exposure of the calcarenite to water vapor.

4.1.2.3 Full-Saturation under vacuum experiment results and discussions

Single-sided and high-field tomograph analyses

Samples fully saturated under high vacuum were weighted by an electronic balance in order to quantify the relative water mass contained into the samples (Table 4.3).

Compound	Sample n°	Specifications	Theoretical Filled Porosity (%)	Theoretical amount (g)
Not treated (reference)	35	-	-	-
	36	-	-	-
	55	-	-	-
Ethyl silicate ESTEL 1000	40	ESTEL 1000, applied 3.2 ml	2.5	0.754
	38	ESTEL 1000, applied 6.4 ml	5	1.508
	39	ESTEL 1000, applied 12.8 ml	10	3.016
	44	ESTEL 1000, applied 12.8 ml	10	3.016
	45	ESTEL 1000, applied 12.8 ml	10	3.016
Nano-Silica	42	Nano-silica 10%, applied 7.54 ml	2.5	0.754
	33	Nano-silica 10%, applied 10.4 ml	3.4	1.04
	41	Nano-silica 10%, applied 15.08 ml	5	1.508
Fluoroelastomer N215	43	N215 at 7% in acetone, applied 15.64 ml	2.5	0.92
	37	N215 at 7% in acetone, applied 33.2 ml	5	1.84
Mix Nano-Silica + N215	52	Mix N215 at 7% in acetone + nano-silica 5%, applied 21.5 ml	2.5	0.812
	50	Mix N215 at 3.5% in acetone + nano-silica 10%, applied 17.0 ml + 6 ml acetone in three times	4.1	1.338

Table 4.4: Masses of samples before and after full-saturation with deionized water.

The reference Maastricht's stone absorbed a mass-relative amount of water of 37 %. It is easy to note that, in all the treated samples, the capability to get water decreases as the product amount increases, confirming that the compound entered in the stone and partially filled the empty space of the pores.

Saturated samples were analyzed by the MOUSE with the same procedure used in the controlled RH experiment. Only the number of scans in the CPMG sequence was considerably decreased from 9000 to 128, taking into account the higher signal-to-noise ratio (SNR) due to the higher amount of water inside the sample. The inversion of the data was made by the software UPEN in order to calculate the transverse relaxation time distributions. Results of the measurement on the reference sample are shown in Fig. 4-9. The blue line refers to the T_2 distribution related to the sample fully saturated, while the black line is related to the sample in the RH=75% condition. Distributions have the same relaxation range, but for the full-saturation condition, most of the signal is concentrated at the longest relaxation times. The distribution is characterized by a main peak centered at around 80 ms with a long tail that reaches the order of hundreds microseconds. The peak is ascribable to the water contained into the largest pores, while the tail is referred to the water restricted in smaller pores.

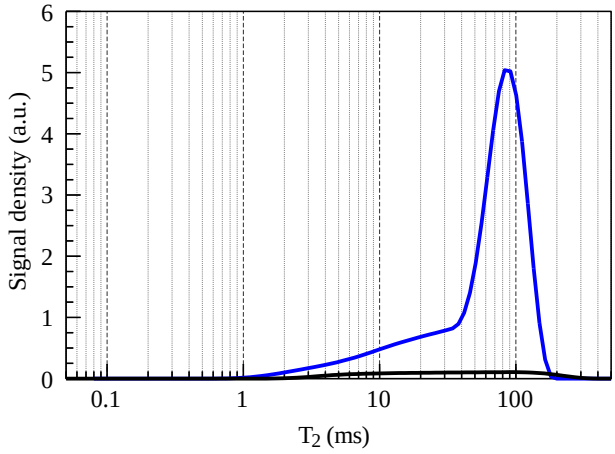

Figure 4.12: Distribution of transverse relaxation times obtained from CPMG data acquired by MOUSE PM 25 for the reference sample. In blue, the distribution of transverse relaxation times for the sample fully-saturated and in black for the sample in condition of RH=75%.

In order to monitor the penetration depth and the distribution of the consolidant inside the stone material [48], [49], each sample was analyzed by the NMR MOUSE PM 25 using a proton density profile procedure [50], and results are shown on the right side of the Figure 4.13. To validate the profile results obtained by the portable NMR probe, the spin-echo imaging data acquired by the superconductor tomograph were evaluated. Intensity values of each pixel column are plotted in order to obtain an intensity profile. As it is possible to note, the water content inside the fully-saturated samples is clearly constant all over the stone, indicating a good penetration and a uniform distribution of the consolidant. Only in the last profile, related to sample treated with the new synthetized compound, is evident the difference of the water content between the first 10 mm and the rest of the stone. This evidence was completely cleared by the MRI analysis using the Varian tomograph. Indeed, looking at the profile obtained from the analysis of the images, the signal intensity of the profile has the same trend of the single-sided probe results and one can link this behavior to a bad distribution of the compound inside the stone. But it is possible to ascribe this behavior to the presence of inhomogeneity of the stone, in particular to the presence of a whole fossil mollusk shell, detectable by the large dark area in the last image in Figure 4.13.

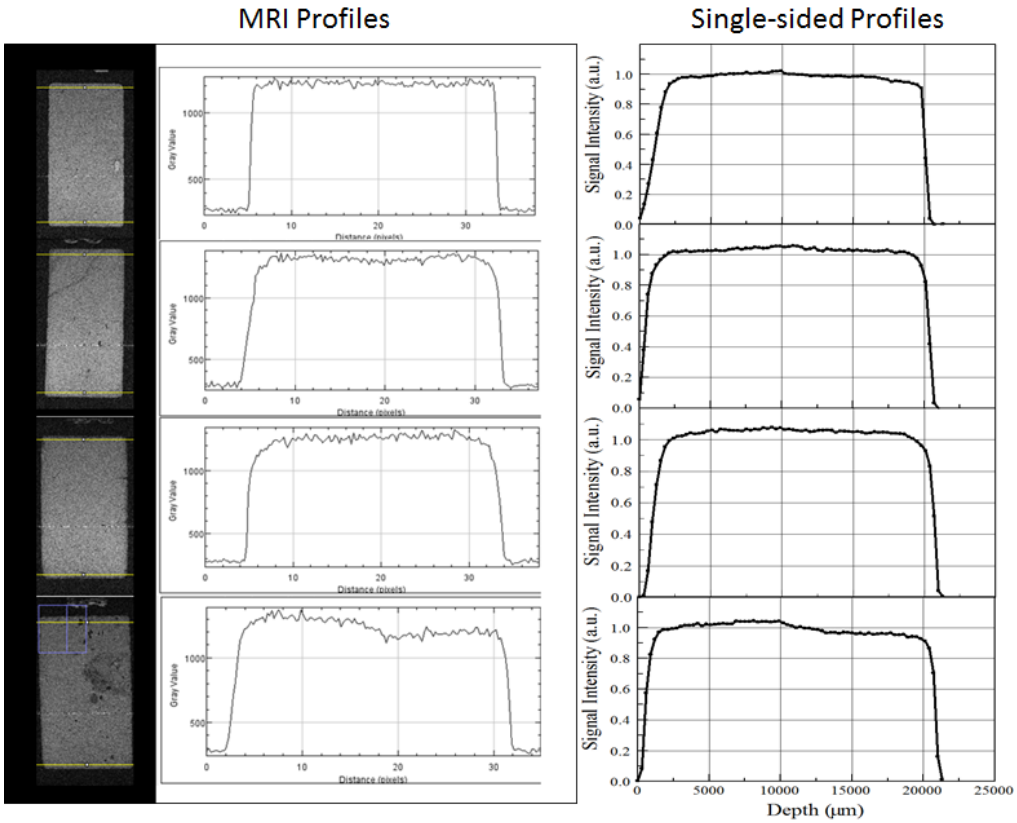

Figure 4.13: from the left: images, profiles obtained by the Varian MRI tomograph, and profiles from NMR-MOUSE PM25. From top to bottom the samples treated with ESTEL, Nano-Silica, Fluoroelastomer, New synthetized compound.

Halbach analysis. The two-dimensional T_2-T_2 relaxation-exchange experiment, performed by the Halbach apparatus, was accomplished by the use of the CPMG-CPMG pulse sequences in order to monitor the connectivity of the pore space after the application of the treatment.

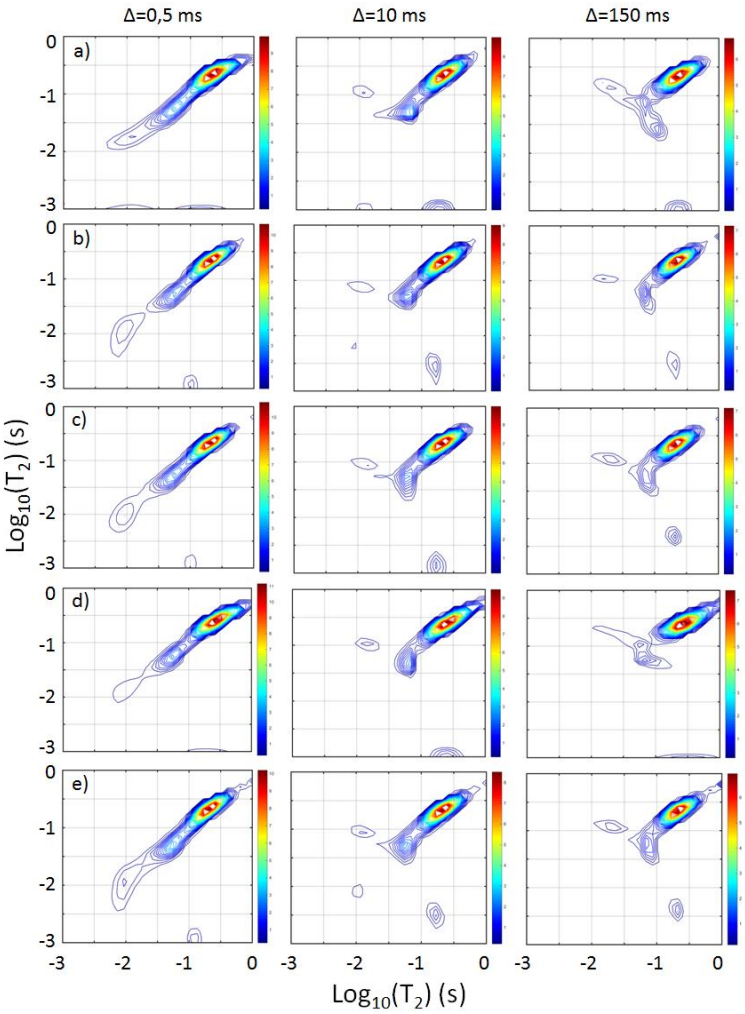

Figure 4.14: T_2-T_2 maps: from left to right increasing mixing time Δ. From top to bottom the different treatments: ESTEL, Nano-Silica, Fluoroelastomer, New synthetized compound.

One of the most important parameter is the mixing time Δ. In Figure 4.14 the results of T_2-T_2 measurements are shown for samples treated with 5% of theoretical filled porosity with a Δ of 0.5 ms, 10 ms and 150 ms. As expected, with the shortest mixing time, 2D

maps of the first column, the shape of the correlation function is symmetrical respect to the main diagonal. As the Δ increases, water molecules have more time for moving from one class of pore to another one, so the probability increases to exchange their magnetizations. Indeed, for Δ = 10 ms and Δ = 150 ms, it is possible to note the formation of off-diagonal peaks and the disappearance of the shortest component on the diagonal. The off-diagonal peaks represent the exchange of magnetization between water molecules belonging to two different sites, one with the transversal relaxation time longer than the other. For each sample it is possible to observe the formation of peaks that show an exchange between water molecules having relation times of around 10 ms and 100 ms. The presence of these peaks in each map with a $\Delta \geq 10$ ms tells us that consolidation treatments, used in this study, do not change the connectivity properties of the stone material, assuring that compounds enter in the stone without a blockage of the pore structure. This is one of the most important characteristic that a conservative treatment must have to be used as a restoration compound for Cultural Heritage.

4.1.2.4 Conclusions

All the consolidative products analyzed showed appropriate characteristics for the use as consolidative agents for the limestone material used in this study. Indeed, compounds have a good capacity to penetrate into the porous medium and they show a uniform distribution inside the stone.

The sample treated with ethyl silicate trapped a considerable quantity of water during the application of the treatment and, in condition of 75% of relative humidity, it absorbed an intermediate amount of water vapor. *Viceversa*, the stone specimen treated with nano-silica did not trap H_2O during the treatment but absorbed the highest amount of water

vapor. The fluoroelastomer has the tendency to snare H_2O molecules during its application and, as a result of its hydrophobic property [51], [39], it captured the minimum amount of water vapor among all the tested compounds. The new synthetized product did not trap the water during the treatment, while the nano-silica did, and, in the controlled relative humidity condition, it absorbed an amount of water vapor intermediate between the values measured for the fluoroelastomer and the nano-silica.

Common consolidants, characterized by hydrophilic properties, absorbed considerable amount, 100-400 mg, of water in condition that well simulate the natural one (75% RH), but the water is one of the main agent that deteriorates the stone material. The attempt to reduce their hydrophilic behavior mixing the fluoroelastomer and the nano-silica showed encouraging results.

All the compounds maintain the connectivity behavior of the stone matrix unchanged as demonstrated by T2-T2 experiment. This is a fundamental characteristic of a conservative compound to be used for Cultural Heritage purposes.

This study has shown how the combination of different NMR techniques, applied in the time domain and spatially resolved, is a powerful approach for the evaluation of the efficiency of consolidative compounds. Furthermore, the comparison between the high-field MRI and low-filed single-sided profile analyses allowed to validate the capability of the portable probe to get robust information for possible in-situ applications.

4.2 Climate Change: effects of Ocean Warming and Acidification on corals

One of the most important environmental issue of our time is the global climate change, that will strongly affect a broad variety of terrestrial and marine lifeforms. It is expected that effects of climate change will influence more the marine communities than terrestrial ones, in particular in temperate areas. The expected increase of temperature is one of the greatest challenge for the marine ecosystems survival, especially for corals. For these reasons, in this work, Mediterranean corals were selected as a natural model for studying the effects on marine calcifying organisms of global climate change, that determines ocean warming and acidification.

TD-NMR, and in particular magnetic resonance relaxometry of water ^{1}H nuclei for analyzing internally connected skeletal porosity, has several advantages compared to other methods because it is a non-destructive and non-invasive procedure, allowing intact specimens to be further analyzed with other techniques. In the studies reported in this thesis, the transverse magnetization component, with transverse relaxation time T_2, was studied. In porous media saturated by water, under the assumptions that the relaxation rate of the unconfined water is negligible and the molecular diffusion is fast enough to maintain the magnetization uniform within the pores, the distribution of T2 corresponds to specific "pore-size" distributions. The area below each distribution is proportional to the total NMR signal and therefore is proportional to the volume of water saturating the skeletal pore volume.

For the first time, the porosity and the pore-space structure of the skeletons of scleractinian corals were analyzed by this technique. In a first experiment, two coral species, *Balanophyllia europaea* (*B. europaea*) (zooxanthellate) and *Leptopsammia*

pruvoti (*L. prouvoti*) (nonzooxanthellate), were taken from three different sites on the western Italian coast along a temperature gradient. In the second experiment *B.europaea* corals were collected along a pH gradient generated by a underwater CO_2 vent located close to the Panarea Island.

The first research has been published with the title "*A Time-Domain Nuclear Magnetic Resonance Study of Mediterranean Scleractinian Corals Reveals Skeletal-Porosity Sensitivity to Environmental Changes*" by P. Fantazzini, S. Mengoli, S. Evangelisti, L. Pasquini, M. Mariani, L. Brizi, S. Goffredo, E. Caroselli, F. Prada, G. Falini, O. Levy, Z. Dubinsky, on *Environmental Science & Technology*, 47: 12679-12686 (2013). The paper and useful references can be found in the online version (doidoi.org/10.1021/es402521b controllare) and/or in the appendix of the printed version of this thesis.

The second research has been published with the title "*Gains and losses of coral skeletal porosity changes with ocean acidification acclimation*" by P. Fantazzini, S. Mengoli, L. Pasquini, V. Bortolotti, L. Brizi, M. Mariani, M. Di Giosia, S. Fermani, B. Capaccioni, E. Caroselli, F. Prada, F. Zaccanti, O. Levy, Z. Dubinsky, J. A. Kaandorp, P. Konglerd, J. U. Hammel, Y. Dauphin, J-P. Cuif, J. C. Weaver, K. E. Fabricius, W. W., P. Fratzl, G. Falini, S. Goffredo, Open Access on *Nature Communications*, 6, Article number: 7785 (p. 1-7). The paper and useful references can be found in the online version (doi:10.1038/ncomms8785) and/or in the appendix of the printed version of this thesis.

The collaboration, project leader for the University of Bologna Stefano Goffredo (Department BiGEA), has involved many international groups from Europe, USA and Israel.

This research has received funding from the European Research Council under the European Union's Seventh Framework Programme (FP7/2007-2013)/ERC Grant 249930 (Coral- Warm: Corals and global warming: the Mediterranean versus the Red Sea).
My personal contribution is related to NMR measurements and analyses, interpreted on the light of all the parameters furnished by the research group.

4.2.1 First experiment: NMR study of corals along the Mediterranean Temperature Gradient

4.2.1.1 Materials and methods

Specimens of *B. europaea L. pruvoti* were randomly collected by SCUBA diving between 1 July 2010 and 4 February 2011 from the three sites, Calafuria (CL), Palinuro (PL) and Pantelleria Isle (PN), along a latitudinal gradient (CL: 43°27'N, 10°21'E; PL: 40°02'N, 15°16'E; PN: 36°45'N, 11°57'E) and a sea surface temperature (*SST*) gradient (CL: 18.84±0.08 °C; PL: 19.72 ±0.07°C; PN: 20.61 ±0.07°C) from the same locations where the porosity of the two species has been studied previously. Coral tissue was totally removed and corals cleaned. Skeletal cleaned dry mass (*m*) was measured with a precision balance. The corals were then placed into a dryer chamber and evacuated by a rotary mechanical pump down to a vacuum of 10^{-2} mbar, and, after 6 hours, water was gently introduced, to fully saturate them. Finally, the pump was switched off and the chamber was vented to the ambient atmosphere. For NMR measurements, the corals were removed from the water container and very rapidly placed on wet paper in order to remove the

excess of water on the external surfaces. Then each specimen was put on the bottom of a glass tube, sealed and measured.

A home-built relaxometer based on a 0.2 T permanent magnet with a coil ≈ 2 cm in diameter in order to analyze the entire coral, without the need to break it into small pieces, and equipped with a Spinmaster console (Stelar, Mede, Pavia, Italy) was used. The Carr-Purcell-Meiboom-Gill (CPMG) sequence with TE=200 μs was used for T_2 relaxation time measurements. Inverse Laplace Transform was performed on relaxation decay data in order to obtain T_2 distributions by the algorithm UPEN (Uniform-Penalty inversion algorithm), implemented in UpenWin software.

The total NMR signal (S_{NMR}), represented by the area below each T_2 distribution, is proportional to the volume of water saturating the pore-space volume V_P. Therefore, one can write $S_{NMR} = kV_P$, where k is a constant depending on instrumental conditions that should be the same for similar specimens. Dividing this signal by the total volume, one gets a value proportional to the total porosity of the specimen (in this case including the empty oral cavity).

Furthermore, the fraction of water with relaxation times over a given interval of the distribution corresponds to the pore volume fraction over a corresponding pore-size range. “NMR macroporosity”, “macroporosity” for short, will indicate the fraction of V_P where the larger pores are weakly coupled by water diffusion to the smaller ones on the local relaxation time scale. If the slope of the distribution shows a strong increase at a certain T_2 value, it is possible to choose this T_2 value as the point of separation between “smaller” and “larger” pores. This relaxation time will be called the “cutoff”. The macro-porosity is then defined as the fraction of ^1H signal with a T_2 larger than the cutoff, divided

by the total ^{1}H signal. Operatively, it is the ratio of the area under the distribution for T_2 larger than the cutoff to the total area under the distribution.

4.2.1.2 Results and discussions

The TD-NMR analysis showed that the distributions of all the coral skeletons are characterized by a major peak at long relaxation times and a long tail, of smaller amplitude, up to three orders of magnitudes wide. The major shape difference between the two coral species was the length of the tail. The major difference among the distributions inside each group was given by the total area, due to the wide range of masses and volumes of the specimens examined. Examples are given in Figure 4.15, along the indication of the "macroporosity" area and a picture of a skeleton.

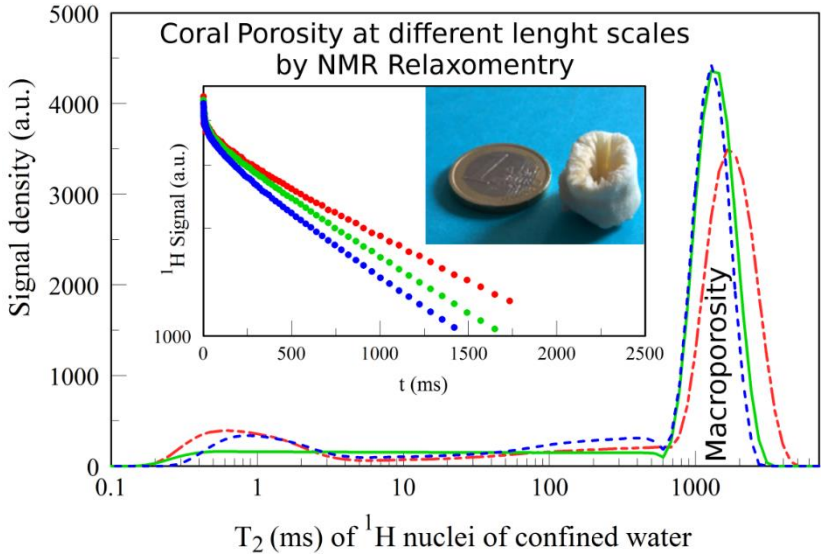

Figure 4.15: Transverse relaxation time distributions of the 1H NMR signal from samples of cleaned coral skeletons, after water saturation of the connected pore space.

In order to discuss the distributions in Figure 4.15 in terms of pore-sizes, a comparison between T_2 distribution and Mercury Injection Porosimetry (MIP) distribution for the same coral skeleton was made. Figure 4.16 reports the MIP distribution for the same specimen. The major fraction of the pore-volume is given by pores whose entrance radius is on the order of tens of µm, while a minor fraction corresponds to a three order of magnitude long tail of very small pores, down to tens of nm. NMR and MPI distributions are exceptionally similar and consistent. The two classes of pores are easily distinguished also in the relaxation time distributions in Figure 4.15. The sharp boundary between the two classes, with a cutoff in the T_2 range 200-400 ms, suggests that the two classes of pores are not well connected. Also, the long tail indicates that these pores are poorly connected both to the other small pores and to the large ones in the major class.

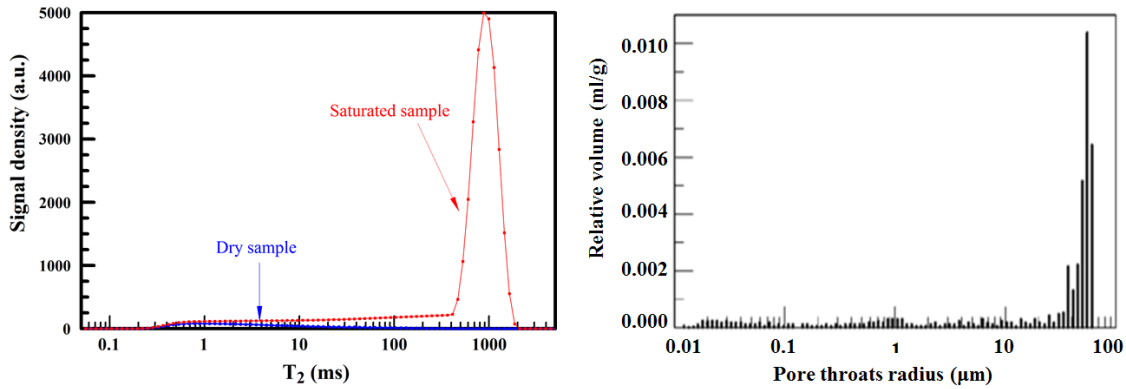

Figure 4.16: On the left, T_2 distribution of a dry coral (blue line) after 1 month in a desiccator and that of the same coral after full water saturation (red line). On the right, the MIP results for the same coral are shown.

The statistical analysis of the correlation among variables (macroporosity, cut-off, mass, Total Volume and NMR signal showed that, significant correlations ($p<0.01$) were found

for pairs variables mass and total volume, mass and SNMR, and total volume and SNMR, in both species. In particular, macroporosity and cut-off, and macroporosity and mass were significantly correlated for both species ($p < 0.01$ for *B. europaea*, and $p < 0.05$ for *L. pruvoti*). More information can be found in the quoted published paper.

The higher the mass, the larger the macroporosity and the longer the cutoff. If the mass increases, both the cutoff and the ratio between the fraction of the two pore classes change, with smallest pores becoming less abundant. This effect is stronger for *B. europaea* than for *L. pruvoti*. This is consistent with the gradual "filling up" of the smaller pores with the growth of the coral.

4.2.1.3 Conclusions

For both species, the sea temperature does not significantly affect mass ($p > 0.1$). A significant relationship between macroporosity and sea surface temperature exists only for *B. europaea* ($p<0.05$). This is consistent with the result of a previous investigation, that showed a dependence of the porosity on the temperature for *B. europaea* but not for *L. pruvoti*. The increase of porosity with temperature in zooxanthellate species

NMR results indicate that this effect could be accompanied by an increase in the fraction of the largest pores in the pore space.

This study shows that TD-NMR is a useful noninvasive and nondestructive method which can be applied to investigate the pore-space architecture of scleractinian corals, measuring differences between species and growing sites, and sensitivity to environmental changes. The results show that TD-NMR parameters are sensitive to changes in the pore structure of the coral skeletons. In particular, a parameter related to the porosity, is larger for *L. pruvoti* than for *B. europaea*, confirming previous non-NMR results. The NMR

macroporosity, describing the fraction of the total pore volume with pore sizes larger than 10−20 μm, has a significant correlation with the mass of the specimen and, for *B. europaea*, with the temperature of the growing site. This phenomenon, that was observed in the zooxanthellate species, could depend on an inhibition of the photosynthetic process at high temperatures that involves an attenuation of calcification. This effect could reduce the resistance to mechanical stresses of the coral, causing possible negative consequences for population density and space colonization.

For these reasons, the effect could have particular importance in determining consequences of global warming on these species.

The TD-NMR method, applied for the first time in this work, has been then applied in a further study concerning the effects of ocean acidification on the skeletal properties of corals, presented in the next section (4.2.2).

About all the details related to the paper published on *Environmental Science and Technology* and references, see the link: dx.doi.org/10.1021/es402521b

4.2.2 Second experiment: Coral skeletal porosity changes with ocean acidification acclimation

Here the TD-NMR method developed in Section 4.2.1 was used to study the acclimation potential of the stony coral *B. europaea* living along a pH gradient caused by a Mediterranean CO_2 vent that serves as a natural long-term experimental setting, located near Panarea Island. A multi-length scale analysis of skeletal features was conducted in parallel to the TD-NMR analysis, exploiting different techniques like Scanning Electron Microscope (SEM) imaging, Micro Computed Tomography (μCT), Nano-indentation, Small Angle X-ray Scattering (SAXS) and Atomic Force Microscope (AFM). The

potentiality of TD-NMR method was to allow the detection of the multi-length scale of the skeleton pore-space by means of a single measurement on the intact skeleton.

4.2.2.1 Materials and Method

The skeletons of 44 corals were analyzed. Corals, of similar age (mean age 12 years), had lived along the CO_2-pH gradient. A 0.2T permanent magnet operating at 8MHz, equipped with a coil ~2cm in diameter, was used for acquisition of the transverse relaxation curve of the ^1H nuclei of water molecules saturating the cleaned coral skeletons. A Spinmaster console (Stelar, Mede, Pavia, Italy) was used for automatic pulse sequence transmission and data acquisition. The transverse relaxation data were acquired by using the CPMG sequence with TE = 200 ms.

The distributions of T_2 were obtained through mathematical inversion of the experimental transverse relaxation curves, as those shown in Figure 4.15. As usual, the ordinate-labeled signal density is an approximation to $dS/(d\ lnT_2)$, where S is the extrapolated signal per Neper (factor of e) of relaxation time. In this study cut-offs were determined in such a way to devide the area under the distribution in nano- micro- and macro-scale pore volume. The nano-, micro-, and macroscale pore volume fractions multiplied by the skeletal porosity (PA), allowed the computation of the TD-NMR nano-, micro-, and macroscale porosities, respectively.

4.2.2.2 Results and discussions

Figure 4.17 shows the TD-NMR results obtained for the 44 coral skeletons in the three selected sites at different pH values.

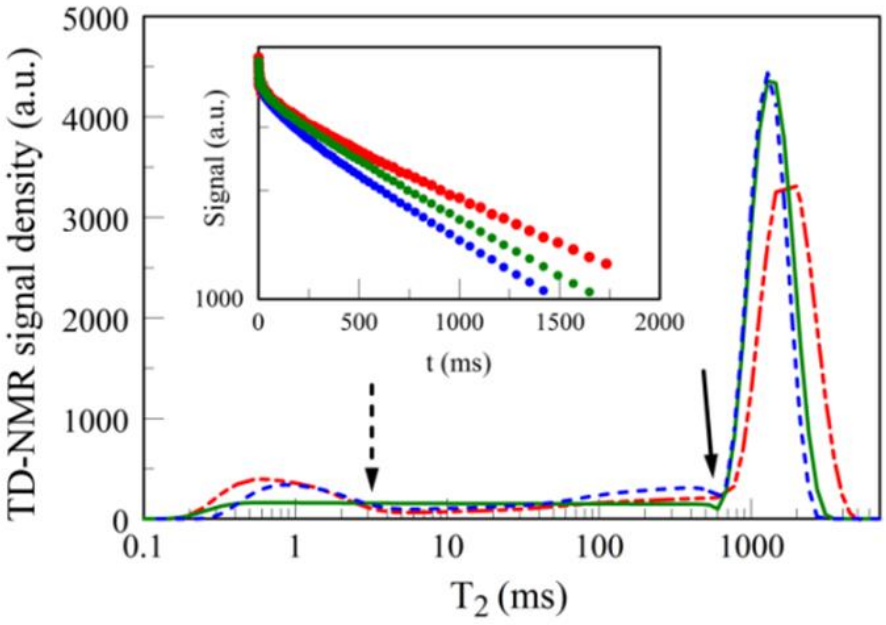

Figure 4.17: Examples of T_2 relaxation time distributions of ^1H NMR signal from cleaned skeletons of B. europaea after water saturation of the connected pore-space.

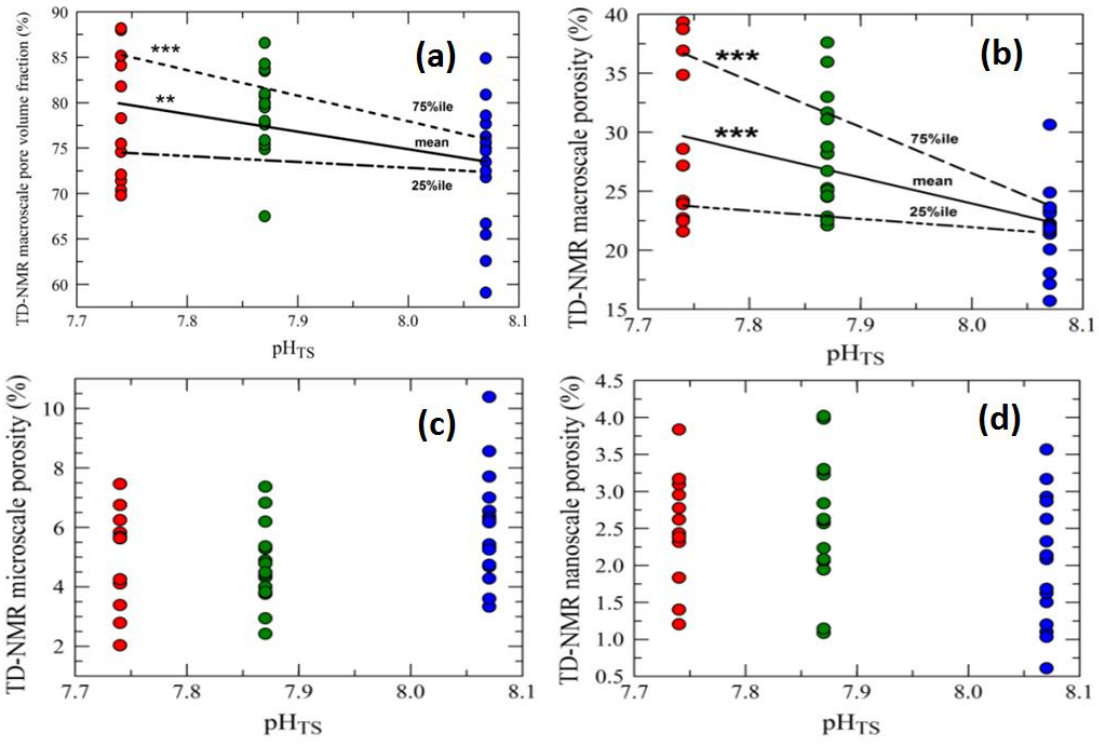

Figure 4.18: a) NMR macro-scale pore volume fraction is reported. c), d) and e) scatterplot reported for the TD-NMR porosities at macro- micro- and nano- for different pH values.

In particular, Figure 4.17 shows the method to determine nano- micro- and macro-porosity. By assuming that the smallest pores have T_2 values smaller than 3 ms, dashed arrow, and the largest pores have T_2 values that exceed the cut-off, solid arrow, three regions can be identified from the T_2 distributions; for simplicity, here they are referred to as nanoscale, microscale, and macroscale pore volumes. The ratios of these pore volumes to the total area under the distribution curve represent the corresponding pore volume fractions. By knowing the porosity of the samples, it was possible to compute the

corresponding contributions to the porosity. Macro-, micro-, and nano-scale porosity are plotted against pH (Total Scale) in Figure 4.18. The sum of macro- micro- and nanoporosity corresponds to the total porosity. The regressions shown in Figure 4.18 a) and *b)* are statistically significant; the regressions shown in *c),* and *d)* are not statistically significant.

One of the most important results was the combination of NMR results with the values of the linear extension rates of the corals obtained by the marinescience group. It was found that this parameter does not vary notwithstanding the increase of macroporosity with increasing acidity of the sea.

4.2.2.3 Conclusions

Weight measurements, combined with TD-NMR data represent a non-destructive technique for determining skeletal porosity over length scales spanning from tens of nanometers to tens of micrometres. Results reported here for *B. europaea* make this species not representative of the generalized response of all coral species to ocean acidification, but they are consistent with observations made on other reef-building scleractinians. as the results show that the skeletal linear extension rate remains constant even if the calcification rates and bulk skeletal density decreases (porosity increases) as functions of reduced aragonite saturation. This phenomenon can be explained by considering an acclimation process of the corals to balance the reduced net calcification rate with an increased macroporosity to maintain constant linear extension. This multi-scale analysis shows that at the nano- and micro-scales, all the skeletal characteristics including biomineral density, are unchanged. Bulk density decrease is dependent on the increase of macroporosity as the pH decrease, while the linear extension rate remains

constant. These observations provide consistent clues regarding the sensitivity of this species to global climate change predicted for the coming decades.

In this study, it has been demonstrated that the almost universally employed measure of coral biomineralization, namely the rate of linear extension, might not be a reliable metric for assessing coral health and resilience in a warming and acidifying ocean. Indeed, in conditions of decreasing seawater pH, although corals tend to acclimate by maintaining linear extension rate and gross skeletal morphology in order to reach sexual maturity, they reduce skeletal resistance to environmental challenges, affecting the long-term survivability of the species.

About all the details related to the paper published on *Nature Communications* and references, see the link:

http://www.nature.com/ncomms/2015/150717/ncomms8785/full/ncomms8785.html

5 ADVANCED APPLICATIONS: HUMAN HEALTHCARE

Whereas everyone knows that NMR can be applied to obtain very important morphological and functional images of human body by MRI, other less known NMR applications can be not less important. Here NMR applications based on the acquisition of NMR signals in the Time Domain will be considered and shown their importance for human healthcare.

In this chapter two examples will be presented. The first one will be the use of single-sided devices to detect the signal locally inside a bone to determine the ratio Bone Volume/Total Volume (BV/TV), an important parameter for osteoporosis diagnosis. The second example will consider the detection and quantification of the morphological changes and water compartmentalization that occur when cells are subjected to stress.

The first research has not yet been published and is still in progress. The second research has been published as "*Water compartmentalization, cell viability and morphology changes monitored under stress by 1H-NMR relaxometry and phase contrast optical microscopy*" by L. Brizi, G. Castellani, P. Fantazzini, M. Mariani, D. Remondini, I. Zironi, *J. Physics D: Applied Physics*, 48: 415401 (9 pp) (2015). The paper and useful references can be found in the online version (http://dx.doi.org/10.1088/0022-3727/48/41/415401) and/or in the appendix of the printed version of this thesis.

5.1 Bone tissue and Osteoporosis

Osteoporosis is a disease characterized by loss of bone tissue, with alterations of bone mineral density (BMD) and architecture, leading to high risk of bone fractures. Dual X-rays Absorptiometry is the gold standard technique, even if it does not measure bone microarchitecture. The importance of assessing bone microarchitecture in addition to BMD for osteoporosis diagnosis has been emphasized in a number of publications.

NMR has been widely applied to assess porosity and pore-size distribution in porous media. Applications have been reported for trabecular bone porosity assessment as well [2], [4], [52], [53]. Here the preliminary results will be reported of a research conducted at the Department DIFA of the University of Bologna, in collaboration with the "Istituto Ortopedico Rizzoli" of Bologna and partially funded by the "*Fondazione del Monte di Bologna e Ravenna*". The goal of the proposal is to establish a new NMR method, based on the use of a mobile NMR single-sided device, for the diagnosis of osteoporosis, through the acquisition of the signal from fingers. The device is mounted on a lift for automatic shift of the magnet in order to get signal from selected internal sensitive volumes, as described in the Section 3.1.1. Here we report the results obtained on animal bone samples built in the shape of cylinders in order to simulate human fingers. Signals have been acquired from four internal sections of the samples and normalized to the signal of bulk marrow samples, in order to determine the ratio Bone Volume to Total volume (BV/TV). The results have been compared with BV/TV obtained by micro-Computed Tomography and a good agreement has been found. These results, based on a new and

original idea, demonstrate the feasibility of the characterization of the microarchitecture of the bone by this method.

5.1.1 Materials and methods

5.1.1.1 NMR measurements

NMR analysis was performed by the single-sided apparatus described in Section 3.1.1 based on the Profile NMR-MOUSE PM10 (Magritek), a portable low magnetic field permanent magnet. In order to characterize the T_1 and T_2 relaxation behaviors, a Saturation Recovery and a CPMG sequences were used. The NMR Profile measurement was executed according to the procedure described in Section 3.1.1 for obtaining a profile related to the proton density of the medium. NMR measurements and analyses were performed at DIFA in collaboration with Marco Barbieri.

5.1.1.2 Micro-Computed Tomography

Samples were analyzed by a Skyscan micro-CT mod. 1072 (Bruker MicroCT, Konthich, Belgium) at the Laboratory of Medical Technology of the Istituto Ortopedico (IOR) Rizzoli of Bologna. The x-ray source was set at 50kV and 200µA with a resolution (pixel size) of 19.54 µm. Each scan was performed with a sample rotation on 180° on its axis, with a rotation step of 0.9° producing 206 projections.

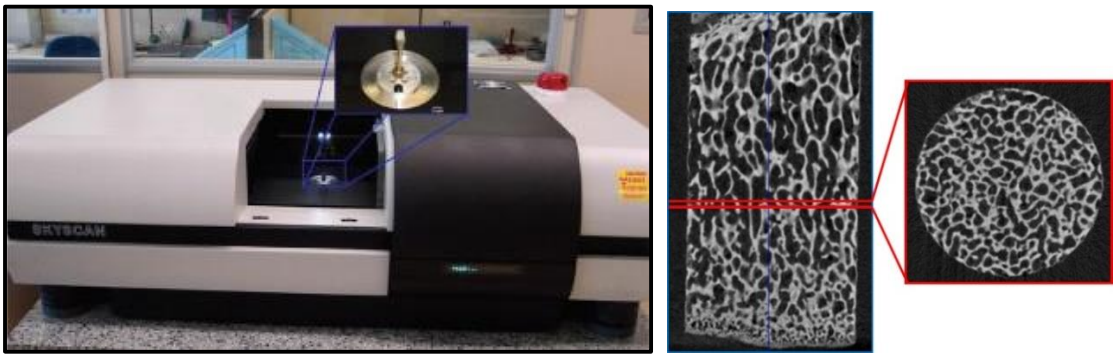

Figure 5.1: Micro-CT Skyscan 1072(on the left). Example of a 2D reconstruction (on the right).

Cross-sectional images were obtained at IOR from the projections by use of NRecon reconstruction software ver. 1.6.8.0 (Bruker MicroCT), with the application of a beam hardening correction of 24% to reduce artifacts. The reconstruction process produced a stack of 997 images in 8-bit bmp format. A global thresholding was applied to binarize the images, and the software CtAnalyser ver. 1.14.4.1 (Bruker MicroCT) was used to calculate the Bone Volume to Total Volume ratio (BV/TV) of the scanned sample. Data acquisition and analysis were performed by Chiara Fersini under the supervision of Fabio Baruffaldi at IOR.

5.1.1.3 Bone samples

Seven samples of pig bone were used. They belong to two different set. The first is a shoulder's pig bone, labelled Bone I, cored in cylindrical shape, of dimensions: diameter 1 cm and height 3 cm. The second set consists of bone samples from different extraction sites of the shoulder's pig. They are labelled as Condilo IB, Condilo IIB, Testa IIA, Testa IIB, SC I SX, SC II SX, Condilo IA. Each sample had a cylindrical shape, with a diameter

of 1 cm and height of 1.5 cm (Figure 5.2). These samples were chosen in order to have samples with a wide range of porosity.

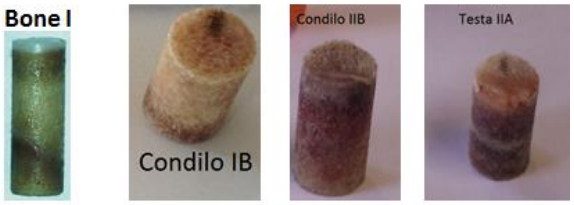

Figure 5.2: Examples of pig bone samples used in the experiment.

5.1.1.4 NMR protocol for the measurement of BV/TV

The sample Bone I was used to determine and optimize the parameters for measurements on the second set of bones. The second set of NMR analysis were performed before micro-CT investigations because it was observed that during micro-CT measurements a loss of NMR signal occurred due to the evaporation of the liquid component. To reduce the duration of the NMR measurements the following protocol was applied on the second set of bones: immediately after coring, the samples were deep frozen. Before NMR, sample were defrosted and left at room conditions for 1 h and 30 min. Then four different CPMG experiments were performed (total time 12 min) with the sample placed horizontally over the MOUSE. By moving the MOUSE with the lift at the suitable position, the CPMG signal was acquired from a sensitive volume located at the depth of 5400 µm, in correspondence of the middle of the sample. The four CPMG experiments were performed after rotating the sample of 90° around its principal axis (Figure 5.3). The average of the four CPMG signals gave the signal intensity of the sensitive volume and the standard deviation the error. Finally, a Profile measurement was accomplished. It

consists of a CPMG experiment repeated at different depths inside the sample. The excited slice thickness of the sensitive volume was 100 µm and the step was set to 500 µm for a total depth of 11.1 mm.

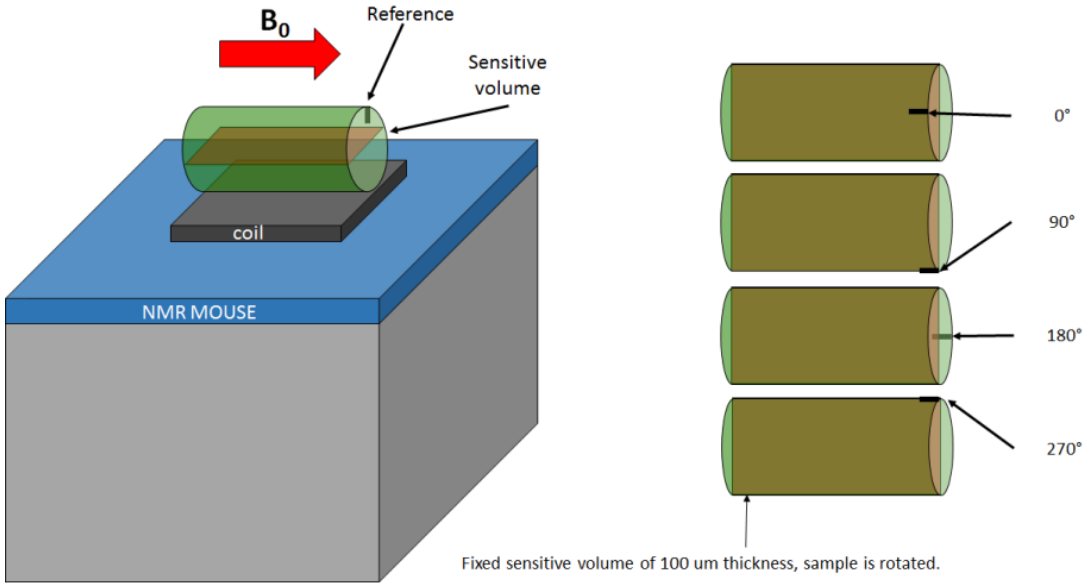

Figure 5.3: Sketch of the setup for four CPMG experiments on bone samples.

The NMR signal is due to the ^{1}H nuclei of the bone marrow inside the trabecular space. Therefore, higher is the signal intensity, higher is the porosity. In order to measure BV/TV the total signal is needed from a sensitive volume fully saturated with bulk marrow. For this reason, bulk marrow samples (without solid component of the bone) were extracted from the tibia of a pig and analyzed in order to determine the total signal of a sensitive volume fully saturated with marrow. From the intensity of the signal obtained from the

marrow of the bone samples, it is possible to calculate the BV/TV parameter in the follow way:

$$BV/TV = (1- S_{bone}/S_{marrow}) \cdot 100\% ,$$

where S_{bone} is the NMR signal from the marrow inside the bone sample and S_{marrow} is the NMR signal from the bulk marrow sample.

5.1.2 Results and discussions

5.1.2.1 Characterization of the bulk marrow sample (without bone)

T_1 distributions were obtained from the saturation recovery measurements. They showed a peak at 75 ms with a tail at longer relaxation times. The T_2 distributions showed a T_2 peak at 30 ms. Figure 5.4 shows the longitudinal and transverse relaxation times distributions obtained. Measurements (data not reported) of the profile measurements on this sample showed that the signal intensity was roughly constant within the marrow.

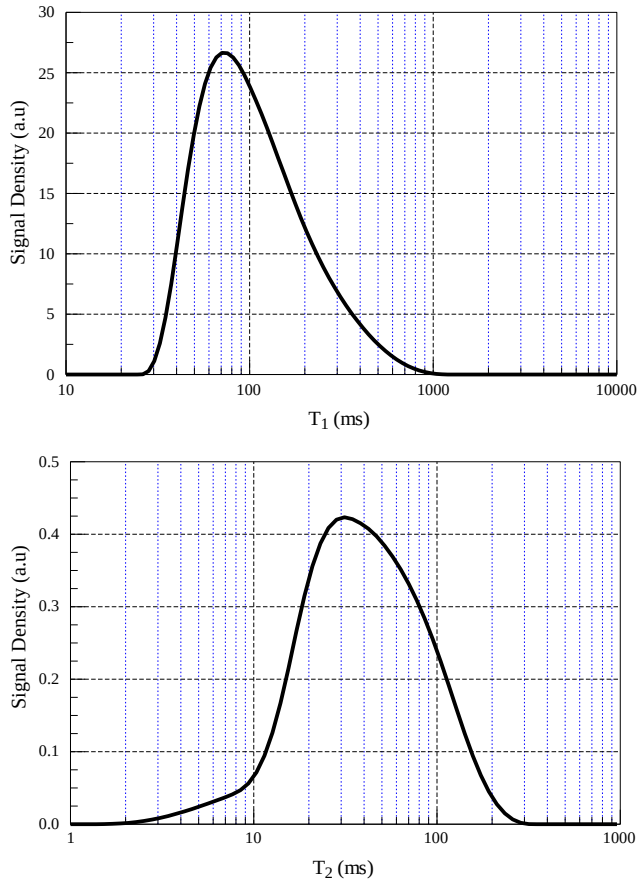

Figure 5.4: T_1 and T_2 distributions of the bulk marrow.

5.1.2.2 Bone I

T_1 and T_2 distributions of the marrow inside the bone in the bone samples are similar to those of the marrow sample. From the profile data it is possible to obtain the percent of the bone marrow present inside the trabecular bone tissue at each depth. To obtain the percent of bone marrow present within Bone I, at each depth, the profile signal coming

from the bone sample was divided by the profile signal coming from the bulk marrow sample (without bone). After normalization to the volume of the samples, the BV/TV parameter at each depth was compared to the values obtained by micro-CT analysis. Figure 5.5 shows the results of the comparison. The values obtained with NMR MOUSE are in good agreement with the ones obtained with the micro-CT technique.

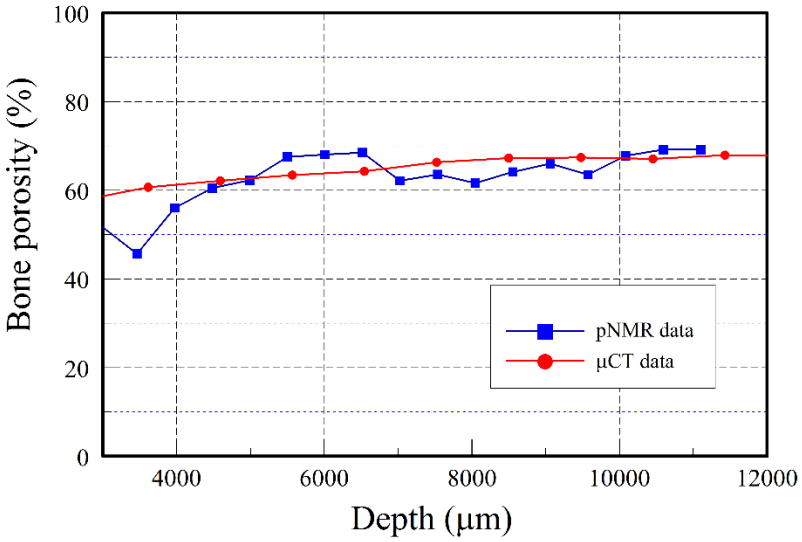

Figure 5.5: Comparison NMR vs micro-TC of the bone marrow percent in function of the depth inside the sample. To compute this NMR parameter, the NMR profile signal from the bone sample was divided by the profile signal coming from the bulk marrow sample (without bone) at the same depth.

5.1.2.3 Second set of Bone samples

Results of NMR analysis on the second set of bone samples were compared with those obtained with micro-CT for the same slices from which the NMR signals were taken. Using the reference markers preliminarily drawn on each sample, and knowing that NMR

signal is obtained from a 100 μm thick slice placed at the depth of 5400 μm inside the sample, for each sample it was possible to perform a micro-CT analysis roughly over the same four slices analyzed with the NMR MOUSE. The micro-CT images of one analyzed slice for three samples are reported in Figure 5.6 as example.

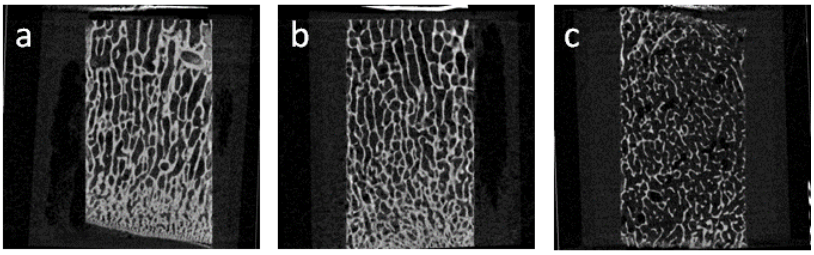

Figure 5.6: Micro-CT image of: a) Condilo IB; b) Condilo IIB; c) Testa IIA;

It is important to remark that growth cartilage is present in some samples. In micro-CT analysis these two tissues can be distinguished, and in principle it is possible to assess the micro-architectural structure of the bone alone and of the cartilage alone, by the selection of a different threshold value for the signal. In NMR analysis, this differentiation cannot be made. The signal comes from the ^{1}H nuclei present both in the inter-trabecular spaces of the bone tissue and inside the growth cartilage. Figure 5.7 shows the NMR signal obtained for the six samples. Table 5.1 shows the comparison of the values of BV/TV determined on the same samples by NMR and by micro-CT, along with the cartilage content (%) as determined by micro-CT.

The comparison shows how in four sample (Condilo IB, Condilo IIB, SC I SX and SC II SX) the difference between the bone volume fraction measured by NMR and by micro-CT is $\leq 4\%$. On the contrary, for Testa IIA and Testa IIB the spread increases up to 10%.

These two samples are extracted from the same body site, i.e. the head of pig's shoulder; in these two samples cartilage is present, moreover Testa IIA has the highest percent of cartilage, and even the highest spread between the two measurement method. The positions in which BV/TV values have been determined by the two methods can differ, moreover we cannot exclude problems deriving for damages in the samples due to the sampling handling in the freezing and thawing of the samples.

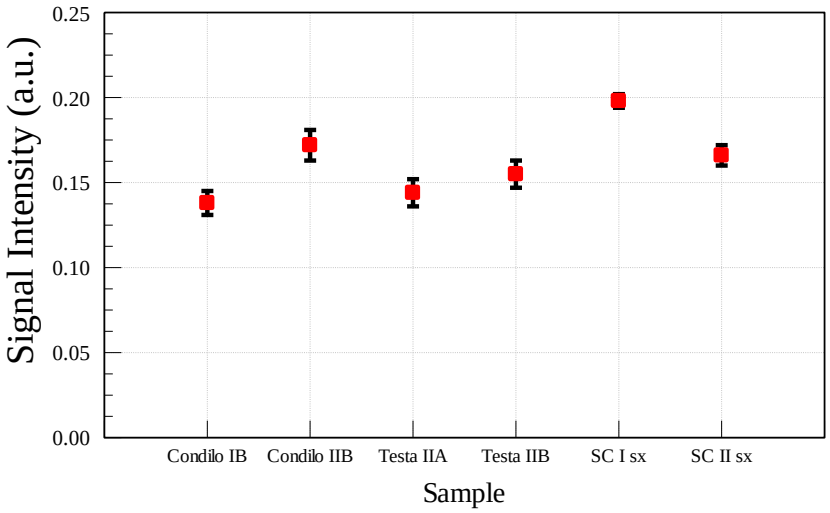

Figure 5.7: Signal intensity, from CPMG data, of the Bone Samples.

Sample	BV/TV by NMR (%)	BV/TV by micro-CT (%)	Cartilage (%)
Condilo IB	47 ± 4	47	19
Condilo IIB	34 ± 6	36	10
Testa IIA	45 ± 5	55	40
Testa IIB	40 ± 5	32	8
SC I SX	24 ± 4	20	0
SC II SX	36 ± 5	35	0

Table 5.1: NMR vs micro-CT. Calculated values of BV/TV

5.1.3 Conclusions

Goal of this project was to determine the feasibility of the determination of bone parameters useful to characterize microarchitecture of trabecular bone by using this innovative low-field, portable, NMR technique. The apparatus has been assembled, tested and a protocol of measurement has been established. The feasibility study of this new NMR-based technique has been realized by determining the BV/TV parameter of six pig bone samples, compared with the micro-CT analysis performed over the same set of samples by the micro-CT scanner at the Istituto Ortopedico Rizzoli of Bologna. The comparison shows a good agreement between the values obtained by the two techniques. In particular, the difference of calculated values of BV/TV by NMR and micro-CT are smaller than 4% in the more homogeneous samples (with low amount of cartilage) for a large range of BV/TV values (20-55%).

These good results have been obtained for a simplified bone model. To make this procedure feasible for clinical purposes further developments are needed. Therefore, for improving and extend the research it is needed (i) to increase the number of the analyzed samples, in order to improve the statistics; (ii) to extend the research to in-vivo

experiments, in order to characterize the signal from tissues different from the trabecular bone tissue, but present in fingers; (iii) to evaluate the possibility to deepen the investigation of the micro-architectural structure of the trabecular bone using relaxation times distributions and 2D NMR relaxometry approaches.

The obtained results demonstrate the feasibility of the method, opening a new way for the diagnosis of osteoporosis, with an apparatus that does not use ionizing radiations, is low-cost and is portable. This last characteristic makes the method eligible for screening of the population at risk of osteoporosis.

5.2 Cellular compartmentalization

Over the years, water compartments, intra-extra cellular water exchange and membrane permeability have been extensively studied in a wide class of tissues and cells with ^{1}H-NMR relaxometry. The measured values for the mean residence times of water in cells depend on measurement conditions and system analyzed. Reported values are 9.8-14 ms for normal human erythrocytes in the range 20-25°C; 40 ms at 37°C for isolated rodent hepatocytes; about 50 ms for F98 glioma cells; in the range 350 ms-1.0 s (from 32°C to 5.0°C) for fresh baker's yeast.

A recent interest for the studies of cellular compartmentalization and water exchange by NMR relaxometry is due to the introduction of paramagnetic contrast agents and magnetic liposomes and nanoparticles, used also in theranostics, to improve the contrast in MRI. These contrast agents change the relaxivity of protons of internal and external water, so that the changed values of the relaxation times improve the contrast in the images. Many of the studies on the effects of contrast agents in cells do not take into account possible

changes in intra-extracellular water exchange over the time after the contrast agent injection.

In this study, the changes of the quasi-continuous distributions of water ^{1}H relaxation times have been analyzed and compared with parallel analysis of phase contrast optical microscopy observations on populations of T98G cells kept up to 400 hours under stress conditions.

5.2.1 Materials and methods

Measurements were performed on glioblastoma multiform cells (T98G), derived from a human tumor. Control measurements were performed on the supplemented culture medium and on a sample of cells pellet insulted by a rotating blade. Details about samples preparations for NMR and phase contrast optical microscopy are available on the quoted article.

NMR measurements were performed with an in-house relaxometer based on a C60 H-L Jeol electromagnet providing a B0=0.473 T static magnetic field, corresponding to a Larmor frequency ~20.15 MHz for the ^{1}H nuclei, equipped with a PC-NMR portable console (Stelar s.r.l., Mede, Pavia, Italy). Measurements for T_1 were performed with an Aperiodic-Pulse-Sequence Saturation Recovery ($\{[\pi/2 + (\pi/2)/10)]_{x10}$ - t_i - $\pi/2$ – FID acquisition$\}$), the comb of ten $[\pi/2 + (\pi/2)/10]$ are used to better kill the signal in the static magnetic field direction. The $\pi/2$ length was 4.1 μs; 64 t_i values were chosen in the range 5 ms – 12 s, logarithmically increasing, to have the same sensitivity in the wide range (up to 4 decades) of relaxation times expected for this kind of samples. Transverse relaxation curves were acquired by a CPMG sequence (TR=12 s, TE=200μs) covering the entire relaxation curve. TE was chosen as short as possible (compatibly with the instrumentation

limits) to reduce the effects of diffusion. NMR measurements were performed at the constant temperature of 24 °C with 8 mm internal diameter glass tubes sealed by Parafilm and 5 mm of sample inside.

The NMR data analysis was performed by inverting the experimental multi-exponential relaxation curves with the inversion algorithm UPEN, implemented in UpenWin software.

5.2.2 Results and discussions

5.2.2.1 NMR Relaxometry results

Identification of intra- and extra-cellular compartments

In order to interpret the distributions of relaxation times of the samples (called CELLS) containing cells and culture medium (CM), preliminary measurements were performed on samples of CM and on a sample of cells previously insulted by a rotating blade in order to damage cells (called HOMOGENATE). Figure 5.8 shows examples of T_1 distributions, representative of all the examined samples, within thirty minutes from sample preparation for a sample of cells, compared with a sample of CM and the sample HOMOGENATE blade Figure 5.9 is the same for T_2 distributions.

The inserts in Figure 5.8 and Figure 5.9 show the experimental curves plotted in semi-log scale. For T_1 they are almost straight lines and gave rise to the mono-modal behavior of the relaxation time distributions. The T_1 distribution for CM is very narrow and centered at about 2.5 s, as expected for a homogeneous solution. The T_1 experimental curve for CELLS sample, that contains cells in suspension in the culture medium, is not mono-exponential and the corresponding T_1 distribution is a wide mono-modal peak, centered

at a shorter time (about 1.5 s). The T_1 distribution of the HOMOGENATE is similar to that of CM, with a wider.

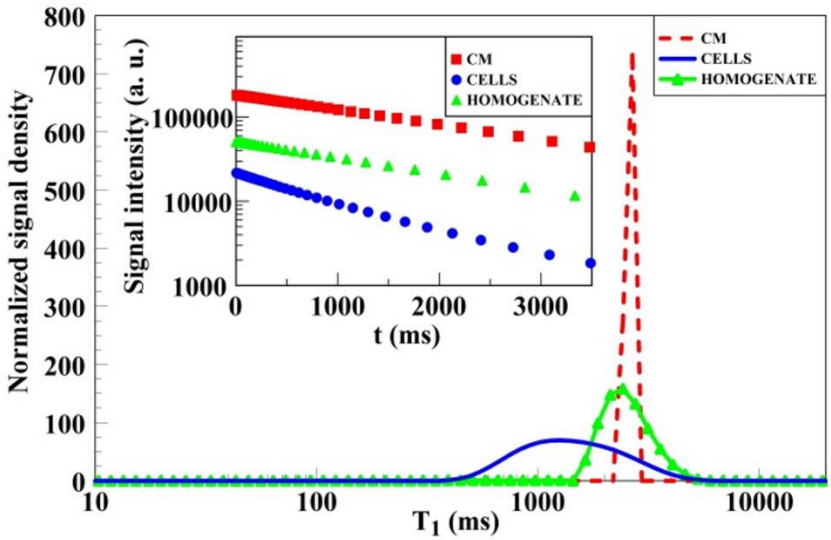

Figure 5.8: Examples of T_1 distributions of the ^{1}H-NMR signal from CM (red, dashed line), CELLS (blue, solid line) and HOMOGENATE (green, dotted line) after ILT of the correspondent relaxation curves shown in the insert. Data were taken within thirty minutes from sample preparation. Results are representative of all the analyzed samples.

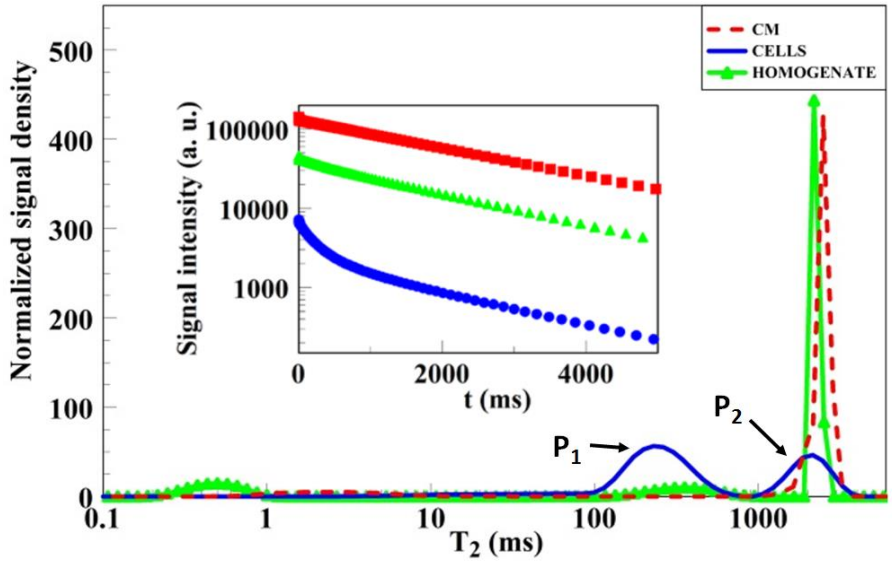

Figure 5.9: Examples of T_2 relaxation time distributions of the same samples of Fig. 5.8, CM (red, dashed line), CELLS (blue, solid line) and HOMOGENATE (green, dotted line) after ILT of the correspondent relaxation curves shown in the inset. Data were taken within thirty minutes from sample preparation. Results are representative of all the analyzed samples.

Figure 5.9 shows the results of the same analysis performed for T_2 of the same samples of Figure 5.8. The experimental relaxation curve for CELLS is clearly multi-exponential and the inversion determines a distribution characterized by two peaks, one centered at about 250 ms, and a second at longer T_2 (~2 s), at about the same position of the main peak of CM.

On the basis of the results on all the three kind of samples, the component at about 250 ms in CELL has been assigned to ^{1}H nuclei of water confined inside the cells. The small feature at about the same value in the HOMOGENATE is likely due to a small amount of cells not disrupted or fragments of them. Therefore, the first peak (P1) has been

reasonably assigned to intracellular protons, mainly due to intracellular water, whose confinement determines a shorter relaxation times, and the second peak (P2) to extracellular protons, mainly due to water molecules in the solution.

The different behavior of T_1 and T_2 can be explained by intra- extracellular exchange of water molecules. From the comparison of the values of intra- and extra-cellular T_2, of the common T_1, and of the relaxation times for the culture medium, it was concluded that the exchange time should be of many seconds. As a conclusion, at least in the first thirty minutes after preparation, the signal amplitudes and relaxation times of the two compartments should not be distorted by the water exchange.

Monitoring cells under stress by transverse relaxation time distributions

The evolution of the two compartments was monitored by the changes of the T_2 relaxation time distributions for about 400 hours, starting from the time of sample preparation. The total signal remained approximately constant overtime. Figure 5.10 shows the evolution of a selection of T_2 distributions obtained at different times on a sample of cells. The same results were obtained in different samples.

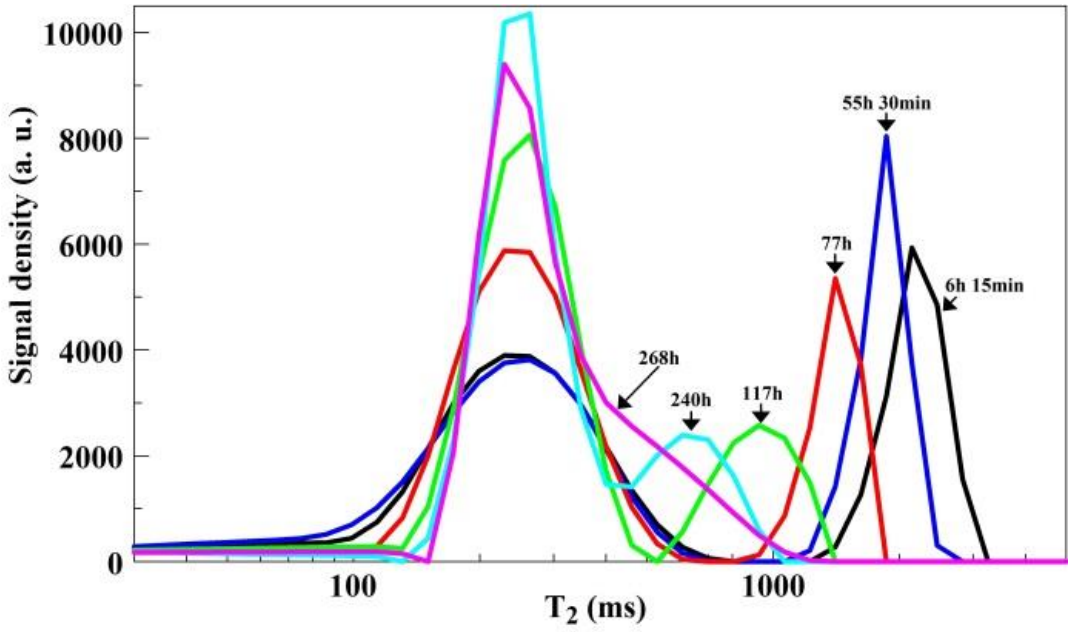

Figure 5.10: A selection of T_2 relaxation time distributions of the ^{1}H-NMR signal from a sample of cells in culture medium at different times after preparation of the sample. It's clear the progressive shift to shorter relaxation times of the distribution related to the compartment assigned to extracellular water (peak at longer T_2). The areas under the distributions are proportional to the signal intensities, proportional to the number of ^{1}H nuclei contributing to the signal. The total area did not change over time.

From the analysis of relaxation times of the two peaks important features were determined. (i) the progressive narrowing of the Full Width at Half Maximum of the peak assigned to the intra-cellular compartment starting from the 40th hour, suggesting an increase of the homogeneity of this compartment; (ii) the insensitiveness of the short-T_2 component over time; (iii) the shift with time of the whole extracellular component

towards shorter times till merging with the values of the intracellular component after about 200 hours.

From the analysis of the relative variations of the weights of the two compartments three main time intervals (phases) can be determined: (i) during the first 40-50 hours there is a monotonic increase (from ~30% to ~40%) of the number of extra-cellular protons at the expenses of the confined ones, maybe due to the water released by the cells under stress and/or dead; (ii) after this first period and until about 100 hours there is a decrease of the weight of P_2 down to ~20%, during this period T_2 of P_2 decreases drastically, while P_1 does not change; (iii) from the 100^{th} hour the weights do not change any more, suggesting that the system has reached a final equilibrium.

These results can be interpreted as a progressive cell membrane disruption because the distinction between intra- and extra-cellular compartments is reduced. Moreover, data suggest the formation of fragmented membranes in which the extracellular fluid can remain snared.

5.2.2.2 Phase contrast optical microscopy results

Analysis of cell population treated with trypan blue for viability monitoring

By this technique it was observed that at the beginning most of the cells are still alive, viable, and are characterized by a light reflection of the cell membrane, differently from the non-viable cells. Then the number of viable cells starts to decrease. It was possible to manually count the viable cells and, as expected, an exponential decay was observed. From the fit to an exponential function from three different experiment, the population half-life was determined and resulted 42 ± 5 h.

5.2.3 Conclusions

The combination of the results obtained by NMR relaxometry and optical observations is depicted in Fig. 5.11.

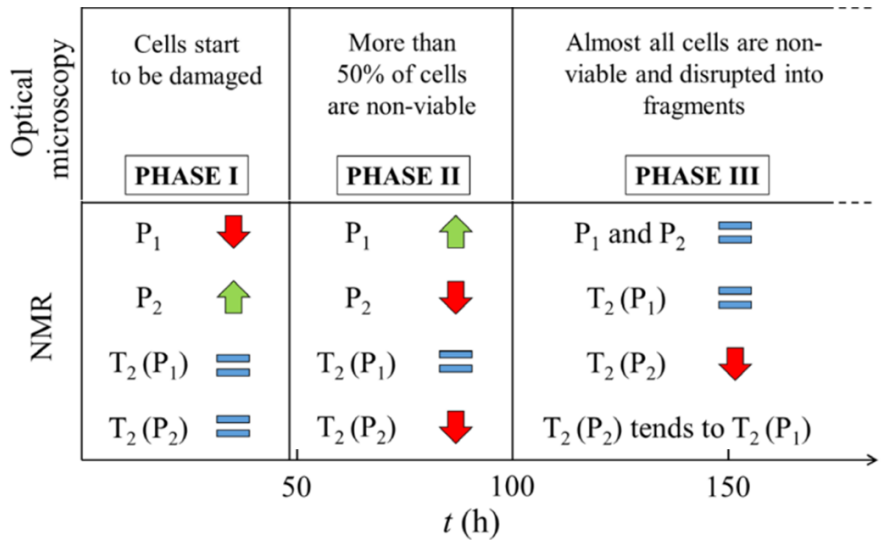

Figure 5.11: Scheme of the comparison of NMR results and optical microscopy observations.

By combining ^{1}H-NMR and optical microscopy it was concluded that the processes related to water exchanges and remodeling of cellular compartments when cells are subjected to stress can be divided into three main phases. In the first phase (up to 40-50h) corresponding to the cell population half-life, as quantified by the optical microscopy, NMR analysis shows that the weight of the NMR peak P1 decrease significantly. Microscopy cannot detect this decrease, which might be due to a progressive modification of cell membranes, with release of intra-cellular water likely through larger membrane pores, but maintaining their integrity. In the second phase, up to 100 h, the number of

cells with damaged membrane becomes larger than the number of undamaged ones with a progressive formation of water bubbles inside cells as observed by optical morphology analysis (images not reported). The trend of the P_1 component is inverted. Probably, while the cell membrane integrity is reduced, the extra-cellular water enters by passive processes and release parts of cell membrane and organelles into extra-cellular space. These fragments could create a confinement for the extra-cellular fluid, causing the observed increase of P_1 component and the shortening of the transverse relaxation time of the P_2 component. After 100 h, most of cells are non-viable. The merging of the two NMR peaks and the constancy of the weights of P_1 and P_2 indicate that the system has reached a final equilibrium.

In conclusion, the comparison of ^{1}H-NMR relaxometry and optical microscopy observations showed good agreement, and validate the use of NMR as a non-destructive, non-invasive technique useful for monitoring modifications of membrane permeability by identifying compartments, following their remodeling and detecting water exchange between them.

6 CONCLUSIONS

In this thesis, time-domain and spatially resolved NMR techniques have been applied to study porous systems of different nature and origin, containing hydrogenous fluids. The unifying principle of this work is showing how the NMR analyses performed with these techniques can be extended to a multiplicity of porous material and how these methods are able to investigate the structure of the pore space and other features in a non-destructive manner, on the intact sample, from the macroscopic scale to the nanometric one. The results of this thesis demonstrates that the same experimental NMR procedures can be successfully applied to perform researches in current important topics that deal with Environment Sustainability and Human Healthcare.

During my doctorate, I exploited for new and advanced applications the expertise developed on porous media by the Bologna NMR research group, about one-dimensional NMR relaxometry and imaging. The most important contributions I have added to the competences of the research group are in the fields of the NMR diffusometry and two-dimensional NMR techniques. I set up new hardware to automatize experiments with the single-sided device, implemented the most recent 2D pulse sequences and supported experimentally the development of a data analysis algorithm for 2D Laplace inversion, based on the 1D ILT UPEN.

A general theoretical framework for the experiments in the field of NMR for fluids in porous media was described at the beginning of this thesis. Relaxation and diffusion processes have been shown to be fundamental phenomena for investigating the structure in terms of pore-size distribution and connectivity of the medium confining fluids. One-dimensional and two-dimensional NMR methods were discussed and their applicability through radiofrequency pulse sequences was tested and then validated.

Relaxometry was applied to the study of coral skeleton modifications due to Ocean Acidification. Skeletal porosity over length scales spanning from tens of nanometers to tens of micrometers was evaluated, giving precious information about the capability of coral to acclimate under adverse conditions (low pH). The results of this study have demonstrated that the almost universally employed measure of coral biomineralization, namely the rate of linear extension, is not a reliable metric for the evaluation of coral health and resilience in a warming and acidifying ocean.

Another application of NMR relaxometry was about the study of water compartmentalization for monitoring viability and morphology changes of cell populations kept under stress conditions. The main result showed that under the experimental conditions considered, three main phases characterize the processes relative to water exchange and remodeling of cellular compartments under stress.

Parallel experiments performed by MRI and NMR single-sided techniques were executed in order to test the efficiency of protectives and consolidants applied for preserving and restore, from the damage caused by atmospheric agents, carbonate building materials of interest to Cultural Heritage. The study confirmed that quantitative MRI and NMR profiles are excellent tools for evaluating the performance of protective compounds. Indeed, traditional methods cannot give information on the spatial distribution of the

protective product on the surface of the internal pore space. They allow to formulate hypotheses that only spatially-resolved NMR can validate. Images and single-sided profiles give localized information about the distribution of the products, as in the case of the accumulation of the fluoroelastomer at the treated surface, and the accumulation of the new synthetized compound SC2-PFPEsol at the untreated face of the sample. This information is of extreme interest to better know the behavior of the products at the interface air-pore surface, in order to improve both the choice of the product and the treatment procedure.

The same approach was adopted to study the performance of consolidant compounds and results have indicated that treatments showed appropriate characteristics for the use as consolidative agents for the limestone material. All the analyzed compounds presented a good capacity to penetrate into the porous medium and they were distributed uniformly inside the stone. NMR relaxometry performed on these samples under controlled RH conditions showed that most common products, ESTEL 1000 and Nano-Silica, absorbed considerable amount of water vapor respect to the untreated sample, due to their hydrophilic nature. The new synthetized compound, a mix of a dispersion of nano-silica particles and a fluoroelastomer, was an attempt to reduce this hydrophilic behavior and revealed encouraging results.

In the course of the study on protective and consolidative compounds, new experimental approaches were developed, with particular attention to the analysis of the apparent diffusion coefficient and the 2D analyses. By the study of the decrease of the apparent diffusion coefficient in samples treated with protective agents as the diffusion time was increased, the reduction of the average pore size could be quantified. Two-dimensional NMR techniques were exploited for investigating the connectivity behavior of the stone

matrix due to the application of consolidative treatments. T_2-T_2 maps confirmed that consolidated samples showed an exchange behavior similar to the not treated one. This was an important result, because it demonstrated that the treatments did not occlude the pore. The conservation of the connectivity is one of the most important characteristic of a compound to be used as a consolidant for Cultural Heritage purposes.

Another porous medium studied was the bone tissue. NMR profile techniques were applied to detect locally the signal inside a bone, to determine the ratio Bone Volume/Total Volume (BV/TV), an important parameter for osteoporosis diagnosis. By single-sided analysis, the BV/TV parameter was determined for six pig bone samples and it was compared with the results of micro-CT analysis. The comparison showed a good agreement between the values obtained by the two different techniques, validating the applicability of this innovative procedure for the diagnosis of the osteoporosis.

The results presented in this thesis demonstrate that time-domain and spatially resolved NMR techniques are excellent tools for investigating the structure of porous materials and the behavior of fluids inside.

Magnetic Resonance for fluids in Porous Media is now a well-established discipline. Even it is not in the mainstream of NMR, its importance is more and more evident, not only for the porous media community, but also for the theoretical and experimental developments that it allows in many different fields. The porous media can be considered as useful models to mimic other systems, not necessarily porous. As a matter of fact, this thesis is as an example of the plenty of information that can be obtained in different systems by experimental setups able to exploit physical phenomena like relaxation, diffusion and their combination. The same theoretical approaches and the same techniques can be applied, for example, to study nerves and muscles.

6 **Conclusions**

Objects of this thesis are systems important for the environmental sustainability and the human health care. The same NMR techniques can be applied to all these system, even if they are so different and belong to so different fields. The unifying principle is given by the fact that in all these systems there are ^{1}H nuclei, that can be subjected to NMR relaxation and to molecular diffusion. The relaxation can be influenced by the walls (solid as in stone or bone, and non-solid, as in cells) and these wall restrict the diffusion. These phenomena make Relaxometry, Diffusometry, Profiling, Imaging, and the 2D techniques unique instruments to study these systems. Moreover, as demonstrated in this thesis, the experiments are performed in a non-destructive way on the intact sample, and give information on the multi-scale lengths of these systems.

7 REFERENCES

[1] P. Fantazzini, "Magnetic resonance for fluids in porous media at the University of Bologna.," *Magn. Reson. Imaging*, vol. 23, no. 2, pp. 125–31, Feb. 2005.

[2] P. Fantazzini, C. Garavaglia, and G. Guglielmi, "From porous media to trabecular bone relaxation analysis: spatial variation of marrow 1H relaxation time distributions detected in vitro by quasi-continuous distribution analysis," *Magn. Reson. Imaging*, vol. 19, no. 3–4, pp. 477–480, Apr. 2001.

[3] P. Fantazzini, R. Viola, S. M. Alnaimi, and J. H. Strange, "Combined MR-Relaxation and MR-Cryoporometry in the study of bone microstructure," *Magn. Reson. Imaging*, vol. 19, no. 3–4, pp. 481–484, Apr. 2001.

[4] P. Fantazzini, F. Galassi, V. Bortolotti, R. J. S. Brown, and F. Vittur, "The search for negative amplitude components in quasi-continuous distributions of relaxation times: the example of 1 H magnetization exchange in articular cartilage and hydrated collagen," *New J. Phys.*, vol. 13, no. 6, p. 065007, Jun. 2011.

[5] L. L. Latour, K. Svoboda, P. P. Mitra, and C. H. Sotak, "Time-Dependent Diffusion of Water in a Biological Model System," *Proc. Natl. Acad. Sci. U. S. A.*, vol. 91, no. 4, pp. 1229–1233, 1994.

[6] M. Gombia, V. Bortolotti, R. J. S. Brown, M. Camaiti, and P. Fantazzini, "Models of water imbibition in untreated and treated porous media validated by quantitative magnetic resonance imaging," *J. Appl. Phys.*, vol. 103, no. 9, p. 094913, 2008.

[7] M. Brai, M. Camaiti, C. Casieri, F. De Luca, and P. Fantazzini, "Nuclear magnetic resonance for cultural heritage.," *Magn. Reson. Imaging*, vol. 25, no. 4, pp. 461–5, May 2007.

[8] M. Camaiti, V. Bortolotti, and P. Fantazzini, "Stone porosity, wettability changes and other features detected by MRI and NMR relaxometry: a more than 15-year study.," *Magn. Reson. Chem.*, vol. 53, no. 1, pp. 34–47, Jan. 2015.

[9] H. C. Torrey, J. Korringa, D. O. Seevers, and J. Uebersfeld, "Magnetic spin pumping in fluids contained in porous media," *Phys. Rev. Lett.*, vol. 3, no. 9, pp. 418–419, 1959.

[10] R. L. Kleinberg and M. A. Horsfield, "Transverse Relaxation Processes in Porous Sedimentary Rock," vol. 19, pp. 9–19, 1990.
[11] G. . Borgia, A. Brancolini, R. J. . Brown, P. Fantazzini, and G. Ragazzini, "Water-air saturation changes in restricted geometries studied by proton relaxation," *Magn. Reson. Imaging*, vol. 12, no. 2, pp. 191–195, Jan. 1994.
[12] G. C. Borgia, R. J. S. Brown, and P. Fantazzini, "Nuclear magnetic resonance relaxivity and surface-to-volume ratio in porous media with a wide distribution of pore sizes," *J. Appl. Phys.*, vol. 79, no. 7, p. 3656, 1996.
[13] C. Casieri, F. De Luca, and P. Fantazzini, "Pore-size evaluation by single-sided nuclear magnetic resonance measurements: Compensation of water self-diffusion effect on transverse relaxation," *J. Appl. Phys.*, vol. 97, no. 4, p. 043901, 2005.
[14] G. C. Borgia, R. J. S. Brown, and P. Fantazzini, "Different 'average' nuclear magnetic resonance relaxation times for correlation with fluid-flow permeability and irreducible water saturation in water-saturated sandstones," *J. Appl. Phys.*, vol. 82, no. 9, p. 4197, 1997.
[15] P. Mitra, P. Sen, L. Schwartz, and Le Doussal P, "Diffusion propagator as a probe of the structure of porous media.," *Phys. Rev. Lett.*, vol. 68, no. 24, pp. 3555–3558, Jun. 1992.
[16] P. P. Mitra, P. N. Sen, and L. M. Schwartz, "Short-time behavior of the diffusion coefficient as a geometrical probe of porous media," *Phys. Rev. B*, vol. 47, no. 14, pp. 8565–8574, 1993.
[17] P. N. Sen, "Time-dependent diffusion coefficient as a probe of geometry," *Concepts Magn. Reson. Part A Bridg. Educ. Res.*, vol. 23, no. 1, pp. 1–21, 2004.
[18] T. M. de Swiet and P. N. Sen, "Time dependent diffusion coefficient in a disordered medium," *J. Chem. Phys.*, vol. 104, no. 1, p. 206, 1996.
[19] Y.-Q. Song, L. Zielinski, and S. Ryu, "Two-Dimensional NMR of Diffusion Systems," *Phys. Rev. Lett.*, vol. 100, no. 24, p. 248002, 2008.
[20] H. C. Torrey, "Bloch Equations with Diffusion Terms," *Phys. Rev.*, vol. 104, no. 3, pp. 563–565, Nov. 1956.
[21] Y.-Q. Song, L. Venkataramanan, M. D. Hürlimann, M. Flaum, P. Frulla, and C. Straley, "T1–T2 Correlation Spectra Obtained Using a Fast Two-Dimensional Laplace Inversion," *J. Magn. Reson.*, vol. 154, no. 2, pp. 261–268, 2002.
[22] A. N. Tikhonov and V. Y. Arsenin, "Solutions of ill-posed problems," in *Physical Review*, V. Winston, Ed. 1977.
[23] B. Blümich, P. Blümler, G. Eidmann, a. Guthausen, R. Haken, U. Schmitz, K. Saito, and G. Zimmer, "The NMR-MOUSE: Construction, excitation, and

applications," *Magn. Reson. Imaging*, vol. 16, no. 5–6, pp. 479–484, 1998.
[24] B. Blümich, J. Perlo, and F. Casanova, "Mobile single-sided NMR," *Prog. Nucl. Magn. Reson. Spectrosc.*, vol. 52, no. 4, pp. 197–269, 2008.
[25] B. Blümich, F. Casanova, J. Perlo, F. Presciutti, C. Anselmi, and B. Doherty, "Noninvasive testing of art and cultural heritage by mobile NMR.," *Acc. Chem. Res.*, vol. 43, no. 6, pp. 761–70, Jun. 2010.
[26] J. Perlo, F. Casanova, and B. Blümich, "Profiles with microscopic resolution by single-sided NMR," *J. Magn. Reson.*, vol. 176, no. 1, pp. 64–70, 2005.
[27] H. Carr and E. Purcell, "Effects of Diffusion on Free Precession in Nuclear Magnetic Resonance Experiments," *Phys. Rev.*, vol. 94, no. 3, pp. 630–638, May 1954.
[28] S. Meiboom and D. Gill, "Modified Spin-Echo Method for Measuring Nuclear Relaxation Times," *Rev. Sci. Instrum.*, vol. 29, no. 8, p. 688, 1958.
[29] J. E. Tanner, "Use of the Stimulated Echo in NMR Diffusion Studies," *J. Chem. Phys.*, vol. 52, no. 5, p. 2523, 1970.
[30] L. J. Zielinski and M. D. Hürlimann, "Probing short length scales with restricted diffusion in a static gradient using the CPMG sequence," *J. Magn. Reson.*, vol. 172, no. 1, pp. 161–167, 2005.
[31] K. E. Washburn and P. T. Callaghan, "Tracking pore to pore exchange using relaxation exchange spectroscopy.," *Phys. Rev. Lett.*, vol. 97, no. 17, p. 175502, Oct. 2006.
[32] M. Van Landeghem, A. Haber, J.-B. D'espinose De Lacaillerie, and B. Blümich, "Analysis of multisite 2D relaxation exchange NMR," *Concepts Magn. Reson. Part A*, vol. 36A, no. 3, pp. 153–169, Jun. 2010.
[33] M. D. Hürlimann, "Diffusion and relaxation effects in general stray field NMR experiments.," *J. Magn. Reson.*, vol. 148, no. 2, pp. 367–378, 2001.
[34] M. . Hürlimann and L. Venkataramanan, "Quantitative Measurement of Two-Dimensional Distribution Functions of Diffusion and Relaxation in Grossly Inhomogeneous Fields," *J. Magn. Reson.*, vol. 157, no. 1, pp. 31–42, 2002.
[35] M. F. Striegel, E. Bede Guin, K. Hallett, D. Sandoval, R. Swingle, K. Knox, F. Best, and S. Fornea, "Air pollution, coatings, and cultural resources," *Prog. Org. Coatings*, vol. 48, no. 2–4, pp. 281–288, Dec. 2003.
[36] H. Cai and X. Liu, "Freeze-thaw durability of concrete: ice formation process in pores," *Cem. Concr. Res.*, vol. 28, no. 9, pp. 1281–1287, Sep. 1998.
[37] L. A. Rijniers, L. Pel, H. P. Huinink, and K. Kopinga, "Salt crystallization as damage mechanism in porous building materials--a nuclear magnetic resonance

study.," *Magn. Reson. Imaging*, vol. 23, no. 2, pp. 273–6, Feb. 2005.

[38] S. J. Haneef, J. B. Johnson, C. Dickinson, G. E. Thompson, and G. C. Wood, "Effect of dry deposition of NOx and SO2 gaseous pollutants on the degradation of calcareous building stones," *Atmos. Environ. Part A. Gen. Top.*, vol. 26, no. 16, pp. 2963–2974, Nov. 1992.

[39] G. C. Borgia, M. Camaiti, F. Cerri, P. Fantazzini, and F. Piacenti, "Hydrophobic Treatments for Stone Conservation - Influence of the Application Method on Penetration, Distribution and Efficiency," *Stud. Conserv.*, vol. 48, no. 4, pp. 217–226, Dec. 2003.

[40] F. Piacenti, "Chemistry for the conservation of the cultural heritage," *Sci. Total Environ.*, vol. 143, no. 1, pp. 113–120, Mar. 1994.

[41] L. Venkataramanan, Y. Q. Song, and M. D. Hürlimann, "Solving Fredholm integrals of the first kind with tensor product structure in 2 and 2.5 dimensions," *IEEE Trans. Signal Process.*, vol. 50, no. 5, pp. 1017–1026, 2002.

[42] "UNI-EN 15801-2010. Conservation of cultural property – Test methods. Determination of water absorption by capillarity," 2010.

[43] E. Casazza, A. Mariani, L. Ricco, and S. Russo, "Synthesis, characterization, and properties of a novel acrylic terpolymer with pendant perfluoropolyether segments," *Polymer (Guildf).*, vol. 43, no. 4, pp. 1207–1214, Feb. 2002.

[44] D. R. Iyengar, S. M. Perutz, C.-A. Dai, C. K. Ober, and E. J. Kramer, "Surface Segregation Studies of Fluorine-Containing Diblock Copolymers †," *Macromolecules*, vol. 29, no. 4, pp. 1229–1234, Jan. 1996.

[45] S. Siegesmund, T. Weiss, and A. Vollbrecht, *Natural stone, weathering phenomena, conservation strategies and case studies.* Geological Society Special Publications No. 205 2002. The Geological Society, London, ISBN 1-86239-123-8.

[46] G. C. Borgia, R. J. Brown, and P. Fantazzini, "Uniform-penalty inversion of multiexponential decay data.," *J. Magn. Reson.*, vol. 132, no. 1, pp. 65–77, May 1998.

[47] G. . Borgia, R. J. . Brown, and P. Fantazzini, "Uniform-Penalty Inversion of Multiexponential Decay Data," *J. Magn. Reson.*, vol. 147, no. 2, pp. 273–285, Dec. 2000.

[48] V. Bortolotti, M. Camaiti, C. Casieri, F. De Luca, P. Fantazzini, and C. Terenzi, "Water absorption kinetics in different wettability conditions studied at pore and sample scales in porous media by NMR with portable single-sided and laboratory imaging devices.," *J. Magn. Reson.*, vol. 181, no. 2, pp. 287–95, Aug. 2006.

[49] M. Camaiti, C. Casieri, F. De Luca, P. Fantazzini, and C. Terenzi, "The Use of Portable Single-Sided Relaxometry and Laboratory Imaging NMR Devices in Stone Conservation," *Stud. Conserv.*, Jul. 2013.

[50] E. Danieli and B. Blümich, "Single-sided magnetic resonance profiling in biological and materials science," *J. Magn. Reson.*, vol. 229, pp. 142–154, 2013.

[51] G. C. Borgia, M. Camaiti, F. Cerri, P. Fantazzini, and F. Piacenti, "Study of water penetration in rock materials by Nuclear Magnetic Resonance Tomography: hydrophobic treatment effects," *J. Cult. Herit.*, vol. 1, no. 2, pp. 127–132, Jun. 2000.

[52] R. J. S. Brown and P. Fantazzini, "Conditions for initial quasilinear T 2 − 1 versus τ for Carr-Purcell-Meiboom-Gill NMR with diffusion and susceptibility differences in porous media and tissues," *Phys. Rev. B*, vol. 47, no. 22, pp. 14823–14834, Jun. 1993.

[53] G. C. Borgia, R. J. S. Brown, and P. Fantazzini, "Scaling of spin-echo amplitudes with frequency, diffusion coefficient, pore size, and susceptibility difference for the NMR of fluids in porous media and biological tissues," *Phys. Rev. E*, vol. 51, no. 3, pp. 2104–2114, Mar. 1995.

Further useful references about Subchapters 4.2 and 5.2 can be found in papers:
Subchapter 4.2:

1. Fantazzini P, Mengoli S, Evangelisti S, Pasquini L, Mariani M, Brizi L, et al. A time-domain nuclear magnetic resonance study of mediterranean scleractinian corals reveals skeletal-porosity sensitivity to environmental changes. Environ Sci Technol. 2013;47(22):12679–86.
2. 1. Fantazzini P, Mengoli S, Pasquini L, Bortolotti V, Brizi L, Mariani M, et al. Gains and losses of coral skeletal porosity changes with ocean acidification acclimation. Nat Commun [Internet]. 2015;6:7785. Available from: http://www.nature.com/doifinder/10.1038/ncomms8785

Subchapter 5.2:

1. Brizi L, Castellani G, Fantazzini P, Mariani M, Remondini D, Zironi I. Water compartmentalization, cell viability and morphology changes monitored under stress by ^{1}H-NMR relaxometry and phase contrast optical microscopy. J Phys D Appl Phys [Internet]. IOP Publishing; 2015;48(41):415401.

ACKNOWLEDGEMENTS

It is my pleasure to thank to whom have contributed to this work.

A special thanks to Prof. Paola Fantazzini for her constant support, guidance and motivation throughout these years.

About specific collaborations, I thank to:

- Cultural Heritage:
  - Dr. Mara Camaiti for the contribution related to the preparation, synthesis and application of treatments.
  - Prof. Villiam Bortolotti for the assistance in the MRI measurements on protective compounds.
  - Dr. Sabina Haber-Pohlmeier for the support in NMR experiments on samples treated with consolidants.
- Climate Change:

  All the coauthors of papers:
  - Fantazzini P, Mengoli S, Evangelisti S, Pasquini L, Mariani M, Brizi L, et al. A time-domain nuclear magnetic resonance study of Mediterranean scleractinian corals reveals skeletal-porosity sensitivity to environmental changes. Environ Sci Technol. 2013;47(22):12679–86.
  - Fantazzini P, Mengoli S, Pasquini L, Bortolotti V, Brizi L, Mariani M, et al. Gains and losses of coral skeletal porosity changes with ocean acidification acclimation. Nat Commun. 2015;6:7785.

The research leading to these results has received funding from the European Research Council under the European Union's Seventh Framework Programme (FP7/2007–2013)/ ERC grant agreement n° 249930—CoralWarm: Corals and global warming: the Mediterranean versus the Red Sea.

- Bone tissue and Osteoporosis:
  - Dr. F. Baruffaldi and Dr. C. Fersini for the supply of bone samples and micro-CT analyses
  - Marco Barbieri for the experimental work, as part of his master's thesis in Physics under my supervision.
  - The "Fondazione del Monte di Bologna e Ravenna" for the partial support to this project, which made possible the acquisition of the NMR console KEA II.
- Cellular compartmentalization
  - All the coauthors of the paper: Brizi L, Castellani G, Fantazzini P, Mariani M, Remondini D, Zironi I. Water compartmentalization, cell viability and morphology changes monitored under stress by ^{1}H-NMR relaxometry and phase contrast optical microscopy. J Phys D Appl Phys.
  - Nico Curti for the help with optical microscopy measurements.
  - Robert James Sidford Brown for useful discussions.

Thanks to all my friends.

Last but not least, a huge thanks to my family!